

# Corner Reflector Deployment for SAR Geometric Calibration and Performance Assessment

UZH-FRM4SAR-TN-100 -- Issue 1.03 – 22.08.2017

ESA Contract No. 4000119113/16/I-EF  
DLR Subcontract No. D / 564 / 67240772



Authors: Adrian Schubert<sup>1</sup>, David Small<sup>1</sup>, Christoph Gisinger<sup>2</sup>,  
Ulrich Balss<sup>3</sup>, Michael Eineder<sup>3</sup>

(1) Remote Sensing Laboratories – University of Zurich, Switzerland

(2) Technical University of Munich, Germany

(3) *Deutsches Zentrum für Luft- und Raumfahrt*, Germany

Distribution List	
Ulrich Balss	DLR-IMF
Michael Eineder	DLR-IMF
Christoph Gisinger	TUM-IAPG
Nuno Miranda	ESA-ESRIN
Adrian Schubert	UZH-RSL
David Small	UZH-RSL

<b>Document Change Record</b>			
<i>Issue</i>	<i>Date</i>	<i>Page(s)</i>	<i>Description of the Change</i>
0.1	10.02.2017		Internal skeleton document
0.2	16.02.2017		Update and comments on skeleton from TUM
0.3	02.03.2017		Comments integrated into skeleton text; highlighting to indicate responsibility; logos added to title page
0.4	17.03.2017		UZH internal revision
0.5	24.03.2017		Some UZH additions; draft contributions by TUM for 3.2.3, 3.3.3 and 4.2
0.6	28.03.2017		Further UZH additions; first draft contributions from UB (DLR) integrated.
0.7	04.04.2017		Further UZH additions
0.8	14.04.2017		Further UZH additions; integration of additional content from DLR
1.0	19.05.2017		UZH completed missing sections; corrected/edited English in sections written by TUM/DLR; generated new Tables 8-11 using intensity- (and not amplitude-) based SCR values, updated discussion accordingly.
1.01	13.07.2017		Document title changed; modified Fig. 1; clarifications added to 3.2.1 (text from TUM); discussion added to 3.5.1 addressing questions related to apparent anomalies in Table 8 (reported by TUM).
1.02	14.08.2017		Added subscript to azimuth angle symbol in Fig. 4 to further distinguish it from incident angle symbol in Eq. 1 and elsewhere; amended Fig. 21 with peak-intensity plot and updated discussion; moved section 3.5 to a new Appendix A as it deals with complex issues not expected to be relevant for some readers; added further discussion to S-1 segment of section 3.5 (now Appendix A) highlighting S-1-specific aspects of the analysis.
1.03	22.08.2017		Edited following comments and suggestions from Matt Garthwaite (GSA). Changes included moving 3.4 to its own section 4, adding clarifications and references.

## **TABLE OF CONTENTS**

<b>1</b>	<b>INTRODUCTION.....</b>	<b>7</b>
1.1	ACRONYMS.....	7
1.2	CONTEXT AND MOTIVATION.....	8
<b>2</b>	<b>CORNER REFLECTORS: THEORETICAL CONSIDERATIONS.....</b>	<b>10</b>
2.1	TYPES OF REFLECTORS.....	10
2.1.1	<i>Characteristics of trihedral corner reflectors</i> .....	11
2.2	SIGNAL TO CLUTTER RATIO.....	11
2.3	GEOLOCATION ACCURACY.....	14
2.4	PLACEMENT AND ORIENTATION.....	17
2.4.1	<i>Reflector placement</i> .....	18
2.4.2	<i>Reflector orientation</i> .....	18
<b>3</b>	<b>CALIBRATION CAMPAIGN: PRACTICAL CONSIDERATIONS .....</b>	<b>20</b>
3.1	TRIHEDRAL CORNER REFLECTOR DESIGN CONSIDERATIONS.....	20
3.2	SURVEYING.....	22
3.2.1	<i>Reference Frames</i> .....	22
3.2.2	<i>DGPS survey</i> .....	22
3.2.3	<i>Terrestrial Geodetic Survey</i> .....	24
3.2.4	<i>Survey protocol sheets</i> .....	27
3.3	CORNER REFLECTOR INSTALLATION.....	28
3.3.1	<i>Equipment and materials</i> .....	29
3.3.2	<i>Corner reflector placement and orientation for time-limited campaigns</i> .....	30
3.3.3	<i>Corner reflector weather protection</i> .....	33
3.3.4	<i>Protection against animals and vandalism</i> .....	35
3.3.5	<i>Field protocol sheet</i> .....	35
3.3.6	<i>Photographic documentation</i> .....	36
<b>4</b>	<b>PRODUCT MONITORING DURING A SAR ACQUISITION CAMPAIGN.....</b>	<b>38</b>
4.1	SENTINEL-1 EXPERIENCE.....	38
4.2	TERRASAR-X EXPERIENCE.....	41
<b>5</b>	<b>PLANNING AND DEPLOYMENT OVERVIEW.....</b>	<b>44</b>
<b>6</b>	<b>CONCLUSIONS.....</b>	<b>45</b>
<b>7</b>	<b>REFERENCES.....</b>	<b>46</b>
	<b>APPENDIX A: SCR AND GEOLOCATION ACCURACY .....</b>	<b>49</b>

## LIST OF TABLES

<b>Table 1:</b> Document acronyms .....	7
<b>Table 2:</b> Values of scaling factor $\alpha$ for different Hamming windows .....	13
<b>Table 3:</b> Theoretical RCS [dBm <sup>2</sup> ] of triangular trihedral corner reflectors ( $\sigma_{\text{triangle, peak}} = 4\pi a^3 \lambda^2$ )..	15
<b>Table 4:</b> RCS [dBm <sup>2</sup> ] of theoretical clutter ( $\sigma_{\text{clutter}} = \beta_0 \cdot 2\rho_a \cdot 2\rho_r$ ) .....	16
<b>Table 5:</b> 3 dB resolution $\rho$ for different TerraSAR-X and Sentinel-1 SLC products .....	16
<b>Table 6:</b> Clutter contribution to ALE [m] ( $\sigma_{\text{CR}} = 3\pi^2 \cdot 1\text{SCR} \cdot \rho_r, a \approx 0.39\text{SCR} \cdot \rho_r, a$ ) .....	17
<b>Table 7:</b> Clutter contribution to phase error [deg] ( $\sigma_{\text{phase}} = 12 \cdot \text{SCR} \cdot \rho_r, a \cdot 180^\circ \pi \text{rad}$ ) .....	17
<b>Table 8:</b> <u>Measured median SCR values</u> [dB] over CRs in Sentinel-1 products, with the number of contributing products (sometimes observed from multiple tracks) in brackets. Values are based on observations at test sites in Switzerland (CH) and the <i>Surat</i> array in Australia (AU). N.B. alignment of the CR boresight with the sensor was only possible to within $\sim 10^\circ$ , esp. over the CH sites. In such cases, the values under-represent the best possible SCR for these target/product combinations by up to $\sim 1$ dB. Values marked N/A are not available. ....	50
<b>Table 9:</b> <u>Theoretical (Theo) and measured (Meas) ALE standard deviation contributions</u> in [m] corresponding to SCR values in previous table, i.e. for Sentinel-1 products. Theoretical values generated using Eq. 3; measured values taken from calibration/validation campaigns over Swiss (CH) and Australian (AU) targets. <b>Red</b> values indicate measured values that are (unexpectedly) <i>better</i> than their theoretical counterparts; <b>green</b> values are equal to or worse than theory (as expected). Values marked N/A are not available. ....	51
<b>Table 10:</b> <u>Boresight-adjusted median SCR values</u> [dB] measured over CRs in S-1 products. Values are based on observations at test sites in Switzerland (CH) and the <i>Surat</i> array in Australia (AU), but have been inflated to roughly compensate for misalignment between the CR boresight and the sensor direction (+1 dB / $10^\circ$ of misalignment). Values marked N/A are not available. ....	52
<b>Table 11:</b> Theoretical geolocation <u>standard deviation contribution</u> in [m] based on SCR values in <b>Table 10</b> , generated using Eq. 3. Values marked N/A are not available. ....	52
<b>Table 12:</b> <u>Mean SCR values</u> [dB] measured over CRs in TSX SSC products, with the number of contributing products in brackets. Values are based on observations at test sites in <b>Germany (DE)</b> and at the Antarctic Peninsula (ANT). Note that boresight alignment was not always possible, so some values under-represent the maximum possible SCR for these target/product combinations. ST-SL = staring spotlight, HR-SL = high-resolution spotlight .....	53
<b>Table 13:</b> <u>Theoretical (Theo) and measured (Meas) ALE standard deviations</u> in [mm] corresponding to SCR values in previous table. Theoretical values generated using Eq. 3 and the nominal ( $\rho_g \times \rho_{az}$ ) resolutions of the TSX SLC products [14]: staring spotlight (0.6 x 0.25 m), high-resolution spotlight (0.6 x 1.1 m). Measured values were taken from calibration/validation experiments over <b>German (DE)</b> and Antarctic (ANT) targets. <b>Green</b> values are equal to or worse than theory (as expected). Values marked N/A are not available. ....	53

## LIST OF FIGURES

- Figure 1:** Appearance of 1.5 m corner reflector in S-1B (a) SM SLC and (b) IW SLC image extracts. The extracts are 70 x 70 samples large, and the target was viewed with a 38.1° local incidence angle in both cases. Yellow crosshairs indicate predicted phase centers (peak intensities) based on the provided annotations and model-based corrections for perturbations (such as atmospheric path delay). The signal to clutter ratio (SCR) was measured to be 3193.3 (35.0 dB) in the SM case (a), and 623.8 (28.0 dB) for the IW product in (b). ..... 8
- Figure 2:** Two UZH 1.5 m corner reflectors in *Torny-le-Grand*, Switzerland, facing ascending and descending S-1 orbits. .... 9
- Figure 3:** Common reflector types used for SAR calibration/validation and their maximum theoretical RCS (a) square trihedral (b) triangular trihedral (c) dihedral (d) top hat (e) sphere.....10
- Figure 4:** Relative RCS reduction off-boresight for corner reflectors, in decibels (dB).....12
- Figure 5:** Definition of areas used during signal to clutter estimation in a SAR image. Modified from [13]. .....14
- Figure 6:** Extract of S-1A orientation calculations for the Swiss *Dübendorf* site at the end of March 2017, generated at <https://www.calsky.com>.....19
- Figure 7:** A CR installed at the Finnish Geodetic Observatory *Metsähovi* in cooperation with DLR. A special tripod base was added to lift the CR above the maximum expected snow level.....20
- Figure 8:** Local weather conditions may require special arrangements. At GARS O’Higgins, Antarctic Peninsula, an additional 1 metre base raised the corner reflector above the winter snow level...21
- Figure 9:** Where applicable, mounting on stable bedrock is a good alternative to a concrete foundation. Example from geodetic observatory *Metsähovi*, Finland. According to recommendations from the Finnish Geodetic Institute (FGI), the stand of the corner reflector was mounted on the 22mm rods. The holes drilled directly into the bedrock (~40 cm deep) were filled with rock epoxy glue manufactured by *Hilti*. (© images by FGI) .....21
- Figure 10:** Reference mark close-ups, with GPS measurement leg placement during survey (a) Reference mark at *Dübendorf*, an easily visible pebble. The orange markings were added to help find the reference mark later (b) Reference mark at *Torny-le-Grand*, where small metal plates had already been implanted in the concrete.....23
- Figure 11:** GPS survey in *Dübendorf* in April 2016 (a) DGPS survey with antenna aligned vertically over reference mark (b) Close-up of integrated bubble level indicating vertical alignment .....24
- Figure 12:** Permanent integration of a corner reflector into a geodetic survey network. A plumb-line is used to mark the vertical footprint of the reflector vertex, where a rod holding a survey prism is mounted in a concrete foundation. Taking into account the vertical offset allows direct survey via the target prism. Image credits to S. Mähler, T. Klügel, BKG.....25
- Figure 13:** Examples of integration of corner reflectors into a local geodetic network (a) measurement of the vertical offset between a survey point and the 1.5 m CR vertex at geodetic observatory in *Wetzell*, Germany (b) installed reflector in *Wetzell* (c) 0.7 m CR installed in Antarctica. Image credits to S. Mähler and T. Klügel, BKG.....26
- Figure 14:** Complete survey protocol for accurate geolocation estimation: the first sheet (top) describes the survey of the reference target (the CR vertex position), the second (at the bottom) describes the associated GPS reference station in global ITRF Cartesian coordinates. ....28
- Figure 15:** Equipment used for accurate CR placement and orientation (a) hand-made corner box for placement into the vertex drainage hole, with weighted plumb line, needle, thread and spring clip; used for precise orientation of the CR vertex over a reference mark (b) Small hole drilled into the corner of the box (c) flathead screwdriver used as a lever to nudge the CR base at mm scale (d) electronic level (e) compass with straight edges that can be aligned with the CR baseplate front-facing edge (f) metal ruler or tape measure for measuring the vertical offset between the CR vertex and the survey mark .....29

- Figure 16:** CR orientation and alignment of the vertex over the reference mark (a) using a compass to align the CR azimuth angle (b) using an electronic level to set the baseplate elevation (c) 2 cm drainage hole at vertex of a 1.5 m reflector (d) threaded corner box in the CR vertex, with clip holding the plumb line (e) plumb line vertically aligned over the survey mark .....31
- Figure 17:** Installed and surveyed reflectors with each vertex aligned vertically over the reference mark, and the boresight axes oriented towards the expected satellite overpass (a) *Torny-le-Grand* 1.5 m (b) *Dübendorf* 1.0 m (c) *Torny-le-Grand* 1.5 m CR pair, oriented towards S-1's ascending and descending orbits.....32
- Figure 18:** Weather-related SCR reduction at Swiss test sites. (a) Water-filled corner reflector at UZH *Dübendorf* site before cleaning on 2016.05.25 (b) at *Dübendorf* during CR drainage on 2016.11.14 (c) at *Torny-le-Grand* on 2017.01.19 after a period of snowfall. Note that (a) and (b) are the same reflector, but the weighting blocks were moved on 2016.05.25 to reduce the possibility of interference from multiple-bounce effects. ....34
- Figure 19:** Trihedral corner reflectors with different types of coverage for weather protection. (a) and (b) show covered reflectors employed by NORUT in Norway using PVC plastic canvas and plexiglass reported to be transparent to radar signals; images from [24], (c) shows a protected reflector at GARS O'Higgins station using a high-frequency transparent Gore-Tex canvas; image by DLR-DFD. ....35
- Figure 20:** Wooden fence in *Wetzell* to keep grazing sheep from the CR .....35
- Figure 21:** Example of a field survey protocol sheet used during the deployment and survey of a CR used for S-1B calibration. The relevant fields were filled in during the survey. ....36
- Figure 22:** Signal to clutter ratio and peak intensity for an S-1A/B time series over Swiss corner reflectors as seen in IW SLC products (a) SCR variation over time (b) relationship between SCR and ALE. Outlier product dates indicated by arrow boxes. All five ALE outliers shown in (b) were confirmed to be caused by rain-filled CRs. The three outliers indicated in (a) were caused by partially snow-filled CRs, although the corresponding ALE was not unusually high. The dotted red line shows the 10 dB SCR threshold applied by UZH for IW SLC products over the *Dübendorf* targets.....39
- Figure 23:** Appearance of triangular trihedral corner reflectors in S-1A/B SLC products for different SCR values. The imagettes were radiometrically auto-scaled, but their contrast relative to background and appearance of sidelobes are visibly correlated to SCR. The yellow crosses represent predicted target positions and are used as plausibility checks during ALE estimation. ....40
- Figure 24:** Time series of the SCR in TerraSAR-X 300 MHz high-resolution spotlight (HS300) images acquired for the reflectors at (a) GARS O'Higgins and (b) *Metsähovi*.....42
- Figure 25:** ALE scatterplot for TSX, corresponding to the data shown in **Figure 24**; (a) GARS O'Higgins (two 0.7m CRs), (b) *Metsähovi* (one 1.5m CR). The red signatures mark the outliers identified by the SCR threshold. The arrow markers point to extreme outliers also identified by the SCR, and which are outside of the plotted axis limits.....43

# 1 INTRODUCTION

## 1.1 Acronyms

Acronyms used in this document are listed in **Table 1**.

**Table 1:** Document acronyms

AGNES	Automated Global Navigation Satellite System Network of Switzerland
ALE	Absolute Location Error
ASAR	Advanced SAR
CHTRF95	Swiss Terrestrial Reference Frame 1995
CLS	<i>Collecte Localisation Satellites</i>
CR	Corner reflector
DEM	Digital Elevation Model
DGPS	Differential Global Positioning System
DLR	<i>Deutsches Zentrum für Luft- und Raumfahrt</i> (German Aerospace Center)
EAP	Elevation Antenna Pattern
EDM	Electronic Distance Measurement
ESA	European Space Agency
ETRF	European Terrestrial Reference Frame
ETRS89	European Terrestrial Reference System 1989
EW	Extended Wide swath (Sentinel-1 acquisition mode)
FRM4SAR	Fiducial Reference Measurements for Synthetic Aperture Radar
GRDH	Ground Range Detected High-resolution
ITRF	International Terrestrial Reference Frame
ITRS	International Terrestrial Reference System
IW	Interferometric Wide swath (Sentinel-1 acquisition mode)
RCS	Radar Cross Section
S-1	Sentinel-1
S-1A/B	Sentinel-1A / Sentinel-1B
SAR	Synthetic Aperture Radar
SCR	Signal to Clutter Ratio
SLC	Single-Look Complex
SM	StripMap (Sentinel-1 acquisition mode)
TOPS	Terrain Observation with Progressive Scans
TDX	TanDEM-X

TSX	TerraSAR-X
TUM	<i>Technische Universität München</i> (Technical University of Munich)
UZH	University of Zurich

## 1.2 Context and Motivation

One of the most important challenges during the calibration/validation phase of a new SAR sensor is the accurate characterisation of the range and azimuth timing. Geometric calibration of the instrument therefore requires empirical determination of the system-inherent range and azimuth biases, which are presumed to be approximately constant over time (at least until a re-calibration is deemed necessary). As described in [38], these two offsets can be understood as mainly instrument-inherent properties.

In the context of sensor calibration, the timing biases characterise the instrument. On the other hand, estimation of the range and azimuth biases at some time *after* calibration can be performed to measure the degree of conformity with the most recent calibration. Such a bias estimation is considered part of instrument or product *validation*.

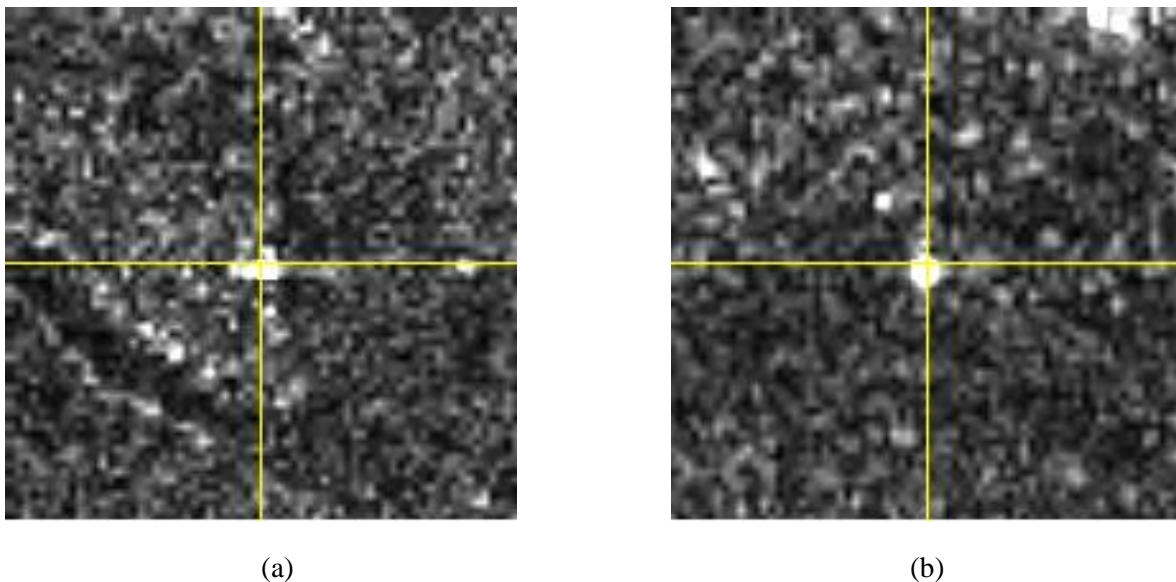


**Figure 1:** Appearance of 1.5 m corner reflector in S-1B (a) SM SLC and (b) IW SLC image extracts. The extracts are 70 x 70 samples large, and the target was viewed with a 38.1° local incidence angle in both cases. Yellow crosshairs indicate predicted phase centers (peak intensities) based on the provided annotations and model-based corrections for perturbations (such as atmospheric path delay). The signal to clutter ratio (SCR) was measured to be 3193.3 (35.0 dB) in the SM case (a), and 623.8 (28.0 dB) for the IW product in (b).

Usually, calculation of the geometric range and azimuth biases is performed using multiple reference targets with accurately known positions, such as passive corner reflectors (CRs) or active transponders. Their global reference positions, determined by geodetic surveying, are transformed into slant-range image coordinates using geolocation (e.g. range-Doppler). These predicted slant range (i.e. radar geometry) coordinates are then compared with the measured intensity peak locations, resulting in a pair of *offset* estimates.

In **Figure 1**, the appearance of a 1.5 m CR in two ascending-orbit Sentinel-1B (S-1B) SLC products is shown, first in a stripmap (SM) mode product with sample dimensions  $rg \times az = 2.66 \times 4.10$  m, and second in an IW mode product having ~3 times coarser azimuth sampling (sample dimensions  $rg \times az = 2.33 \times 13.94$  m). The reflector imaged in **Figure 1** is shown in the foreground in **Figure 2**; it was installed near *Torny-le-Grand*, Switzerland and oriented towards a “mean” ascending orbit for S-1A/B (N.B. the orbits for S-1A and -1B are nearly identical).

In order to perform geolocation measurements suitable for sensor calibration, the deployment and careful survey of one or more reference targets is required. Usually these are CRs, although active transponders, which simulate an

amplified, reflected pulse, may also be used. UZH does not generally recommend the use of transponders for accurate geolocation estimates, as the connection between the imaged peak intensity and the associated position in a geodetic reference frame is influenced by electronic timing biases that may not be well understood. However, the high effective RCS of transponders have been shown to be useful for other applications (e.g. [27]). A campaign based on the use of CRs includes a number of steps, from the acquisition or construction of the targets themselves to site selection, deployment, surveying and maintenance.

The aim of this document is to provide information for stakeholders on the selection of suitable calibration sites and deployment of CRs for an accurate geodetic survey, based on theoretical as well as practical considerations. The document's focus is on spaceborne SAR geometric calibration/validation, and is limited to the experiences gathered by the authors, although a number of references are included for further information beyond the nominal scope of this document. For readers interested in deformation monitoring, an in-depth discussion of theoretical and practical considerations for CR size and design is provided in [17], which complements this report in several ways.

An overview of the recommended procedures to be undertaken is provided in section 5.



**Figure 2:** Two UZH 1.5 m corner reflectors in *Torny-le-Grand*, Switzerland, facing ascending and descending S-1 orbits.

## 2 CORNER REFLECTORS: THEORETICAL CONSIDERATIONS

### 2.1 Types of reflectors

Several common reflector types used for geometric or radiometric calibration are shown in **Figure 3**, along with their maximum theoretical Radar Cross Section (RCS) values [9][20].

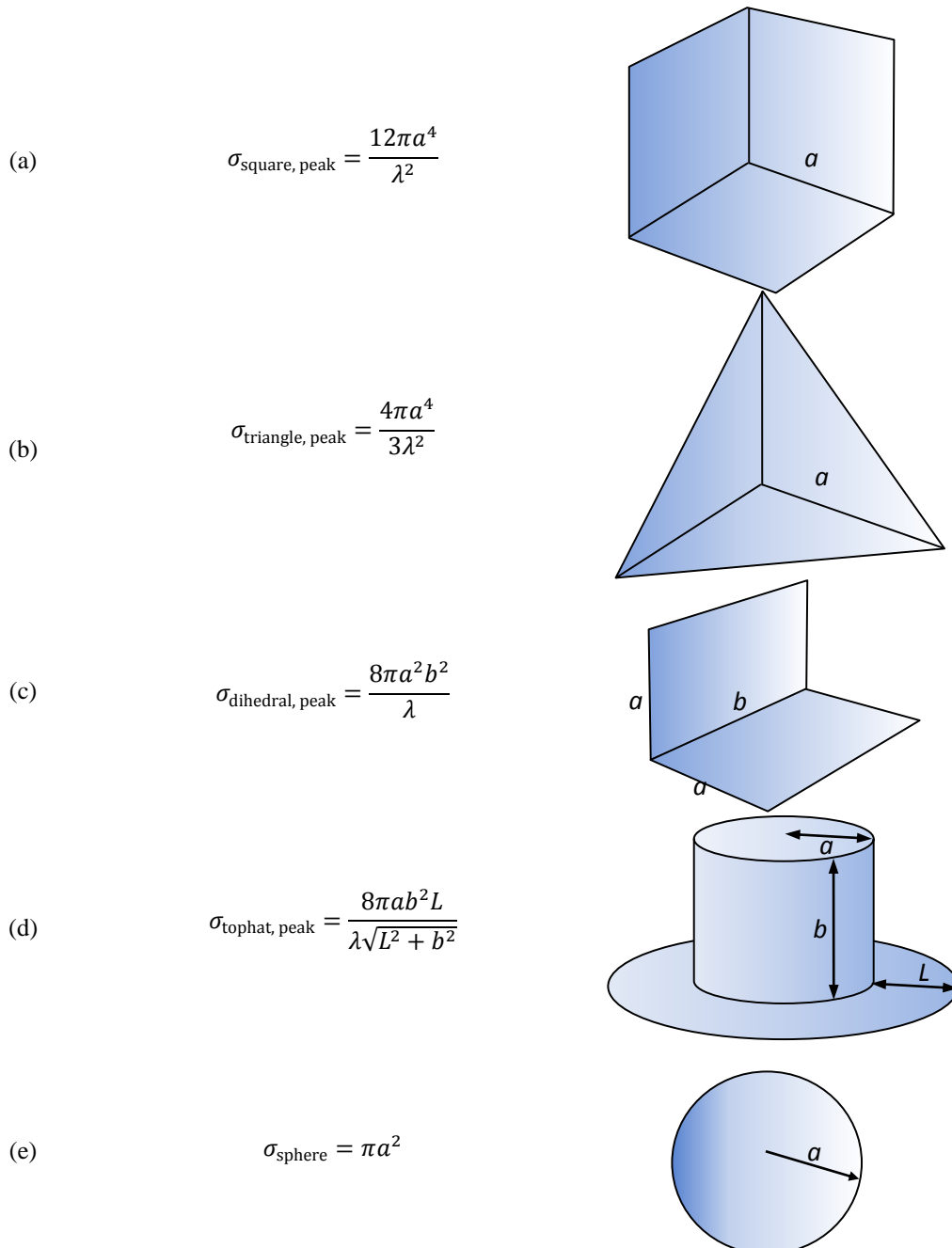


**Figure 3:** Common reflector types used for SAR calibration/validation and their maximum theoretical RCS (a) square trihedral (b) triangular trihedral (c) dihedral (d) top hat (e) sphere

If geometric calibration of the SAR sensor is the sole purpose for deploying the CR, then three important factors are usually considered: (1) the peak RCS (2) the decrease in RCS at off-boresight angles and (3) the ability to accurately measure the physical point corresponding to the peak image intensity (the “phase centre”). The primary goal of the CR in such a scenario is to provide a strong point-target response in the SAR image, with a single, well-

defined peak intensity whose position can be measured in the image. Because of their much stronger signal owing to the triple-bounce mechanism, useful CR designs are generally limited to the trihedral CRs depicted in **Figure 3a** or **b**, while the others may be used under certain circumstances for radiometric calibration. As this report deals only with *geometric* calibration, it concentrates on the use of trihedral CRs. In practice, trihedral CRs are usually the first choice for SAR geometric calibration.

Since measurement of the target peak intensity in a SAR image is more accurate for higher SCR, it is important to consider the reflector placement as well as its physical characteristics when planning a calibration/validation campaign. The reflector's physical "phase centre" position – corresponding to the imaged peak intensity - should also be accessible to accurate measurement during the survey itself. With trihedrals, this is usually a simple task.

### 2.1.1 Characteristics of trihedral corner reflectors

Trihedral CRs (square or triangular), shown in **Figure 3a** and **b**, are often considered the most practical device for calibrating radar systems: they are inexpensive, inherently stable, relatively simple to manufacture and have a high peak RCS along the boresight axis [12], see **Figure 4a**. The relative RCS does not decrease very quickly off-boresight, making it useful in situations where precise alignment of the boresight with the SAR sensor cannot be achieved. Most of the backscatter from a trihedral CR (i.e. corresponding to a 3 dB beamwidth) corresponds to  $\sim 40^\circ$  in both elevation and azimuth off-boresight. This is illustrated in **Figure 4b** and **c** for triangular, and in **Figure 4d** for square trihedral CRs, where the relative RCS is shown as a function of azimuth and elevation angle variation.

The main disadvantage of trihedral reflectors is that in theory, cross-polarised radiation will not be scattered at all by a trihedral (due to destructive interference), limiting its use to co-pol channels (i.e. HH or VV). However, for geometric calibration, this is not generally a problem.

## 2.2 Signal to Clutter Ratio

The signal to clutter ratio (SCR) of an imaged CR can be used as a measure of the suitability of the CR for radiometric calibration/validation. For example, a design requirement on the SCR of 500 in linear intensity units (i.e. 27 dB, computed as  $10 \cdot \log_{10}(500)$ ) may be defined as a desired minimum to guarantee a certain degree of theoretical error (geometric or radiometric). The SCR is defined simply as the ratio between the RCS of the CR and the clutter background, corresponding to the ratio of the square of the amplitudes (i.e. the intensities). In practice, the SCR is generally calculated as the ratio between the peak CR intensity and the mean background intensity (e.g. [13][18][19][22]), and for a SAR SLC image it needs to be projected into range and azimuth coordinates:

$$SCR = \frac{RCS_{CR}}{\sigma_0} \cdot \frac{\sin\theta_i}{\rho_r\rho_a} = \frac{I_{peak}}{I_{meanclutter}} \quad \text{Eq. 1}$$

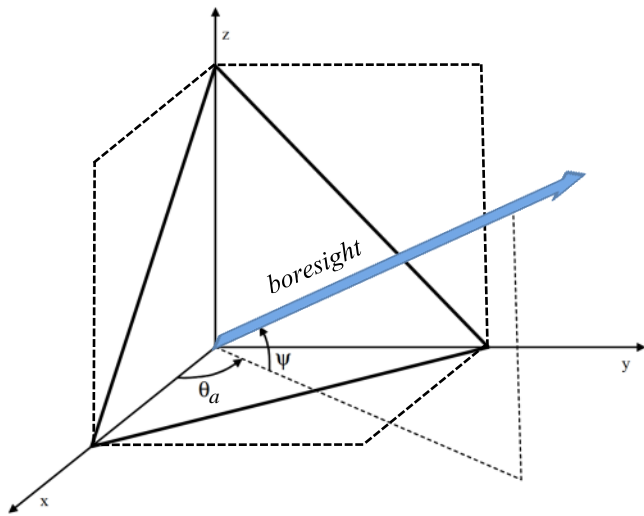
with

$\sigma_0$  = normalised mean RCS of the clutter

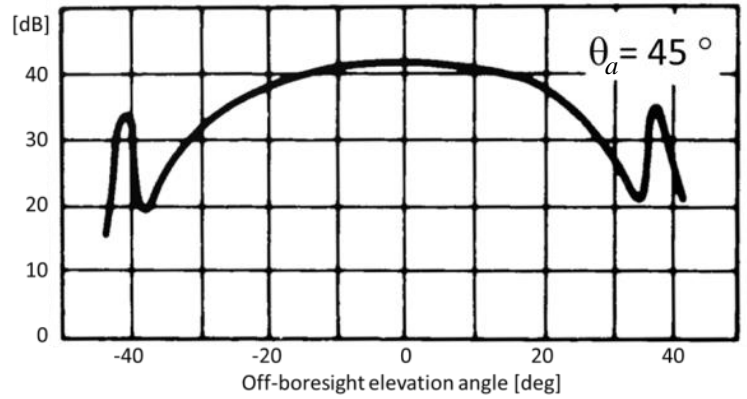
$\theta_i$  = local incident angle

$\rho_r, \rho_a$  = resolution in range and azimuth dimensions

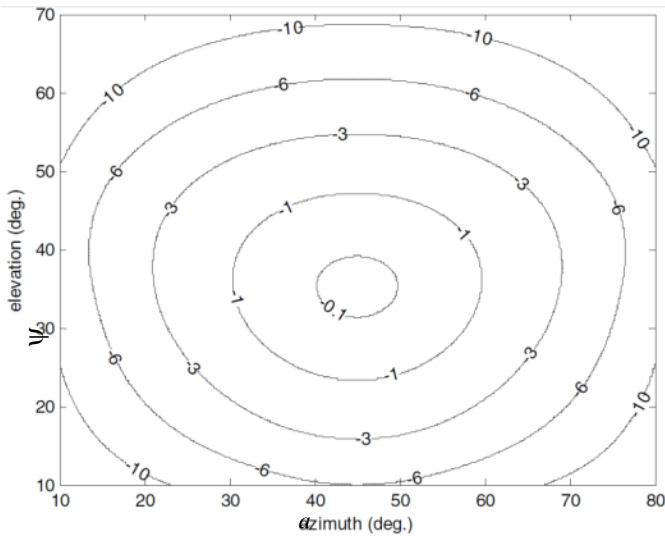
$I$  = intensity of either peak or mean clutter, where  $I = I^2 + Q^2$  for the real and imaginary signal components of the pixels



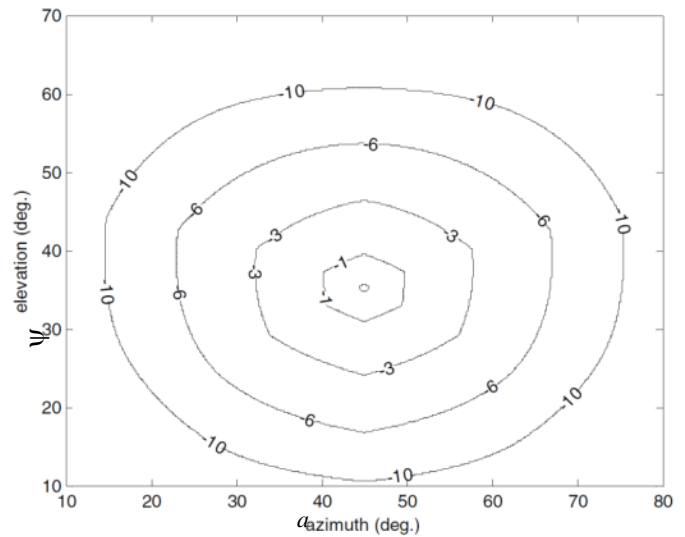
(a)



(b)



(c)



(d)

**Figure 4:** Relative RCS reduction off-boresight for corner reflectors, in decibels (dB); (a) illustrates the angle definitions used in c and d, with dotted lines showing a square trihedral and solid lines a triangular trihedral; the blue arrow indicates the boresight axis, the direction of maximum backscatter (b) off-boresight RCS variation in elevation for a triangular trihedral CR (c) 2-D pattern for a triangular trihedral corner reflector (d) 2-D pattern for a square trihedral corner reflector. (a), (c) and (d) adapted from Figs. 3 – 5 in [9]; (b) adapted from Fig. 7.12 [7].

The resolution  $\rho$  is defined as the 3 dB width of an imaged point target:

$$\rho \approx \alpha \cdot \frac{v}{B} \tag{Eq. 2}$$

with

$v$  = the ground track velocity in the azimuth direction, or  $\frac{c}{2}$  in the range direction

$B$  = target bandwidth (in azimuth or range)

$\alpha$  = factor of proportionality, which depends on the spectral weighting applied in SAR processing.

Spectral weighting using a Hamming window is applied by the standard processor for S-1 and TerraSAR-X (TSX) L1B data products. The dependency of  $\alpha$  on the coefficient of the Hamming window is tabulated in **Table 2**, which lists coefficients used by the operational TSX and S-1 processors.

**Table 2:** Values of scaling factor  $\alpha$  for different Hamming windows

Hamming coefficient	0.5	0.55	0.6 (TSX)	0.65	0.7	0.75 (S-1)	0.8	0.85	0.9	0.95	1
Factor $\alpha$	1.4406	1.2756	1.1692	1.0955	1.0416	1.0004	0.968	0.9417	0.92	0.9018	0.8863

$\sigma_0$  depends on the local background radar response and the wavelength. For X-band, we consider -8 dB to be a reasonable value for typical CR installation sites with low surface roughness and little vegetation present. In Eq. 1, the term  $\frac{\sigma_0}{\sin\theta_i}$  can also be replaced by the radar brightness  $\beta_0$  estimated in the image from the mean clutter intensity.

Several methods have been proposed for the SCR measurement, in particular for the mean clutter intensity [13][18][19][22][29]. The implementation used by UZH for all SAR image products was based on definitions proposed by [13] in the context of radiometric calibration using CRs. A similar method was used by the European Space Agency for radiometric calibration of its ENVISAT ASAR sensor in the past [34]. The general idea is illustrated in **Figure 5**. An imagette is defined surrounding a CR position, as well as areas including the CR signal (including sidelobes), with the remaining pixels within the imagette considered to be pure clutter.

The shape and dimension of the outer imagette is defined differently according to different authors/groups (e.g. [13][18][19][22]), but it cannot be too large, as the SCR estimate is only valid if the clutter intensity corresponds approximately to the clutter at the CR position. The UZH method defines the outer imagette according to a practical computational limit (defined as a maximum permitted number of interpolated samples) in combination with range and azimuth oversampling factors that result in roughly equal ground sample spacings. This is done to ensure approximately equal positional uncertainty in each dimension in the specification of the final peak position. For example, if the azimuth sample interval is four times that of the ground range spacing, then the azimuth oversampling factor is set to be four times as large as well. Fast Fourier Transform (FFT) oversampling is performed using zero-padding to help locate the CR peak intensity location with sub-pixel precision. For a typical S-1 IW SLC product, the range oversampling factor could be 45 and the azimuth oversampling factor 180, with an outer window size for the FFT specified as 1.5x these values along each dimension (resulting in an FFT window of 68 x 270 rg x az samples). In this example, the range precision would be 1/45<sup>th</sup> of a sample (5.2 cm for a 2.33 m sample spacing) and 1/180<sup>th</sup> of an azimuth samples (7.7 cm for a sample spacing of 13.94 m). For all S-1 ALE estimates discussed in this report (made by UZH), the maximum permissible number of oversampled grid positions was set to 8192 (e.g. 45 x 180 = 8100, near the maximum).

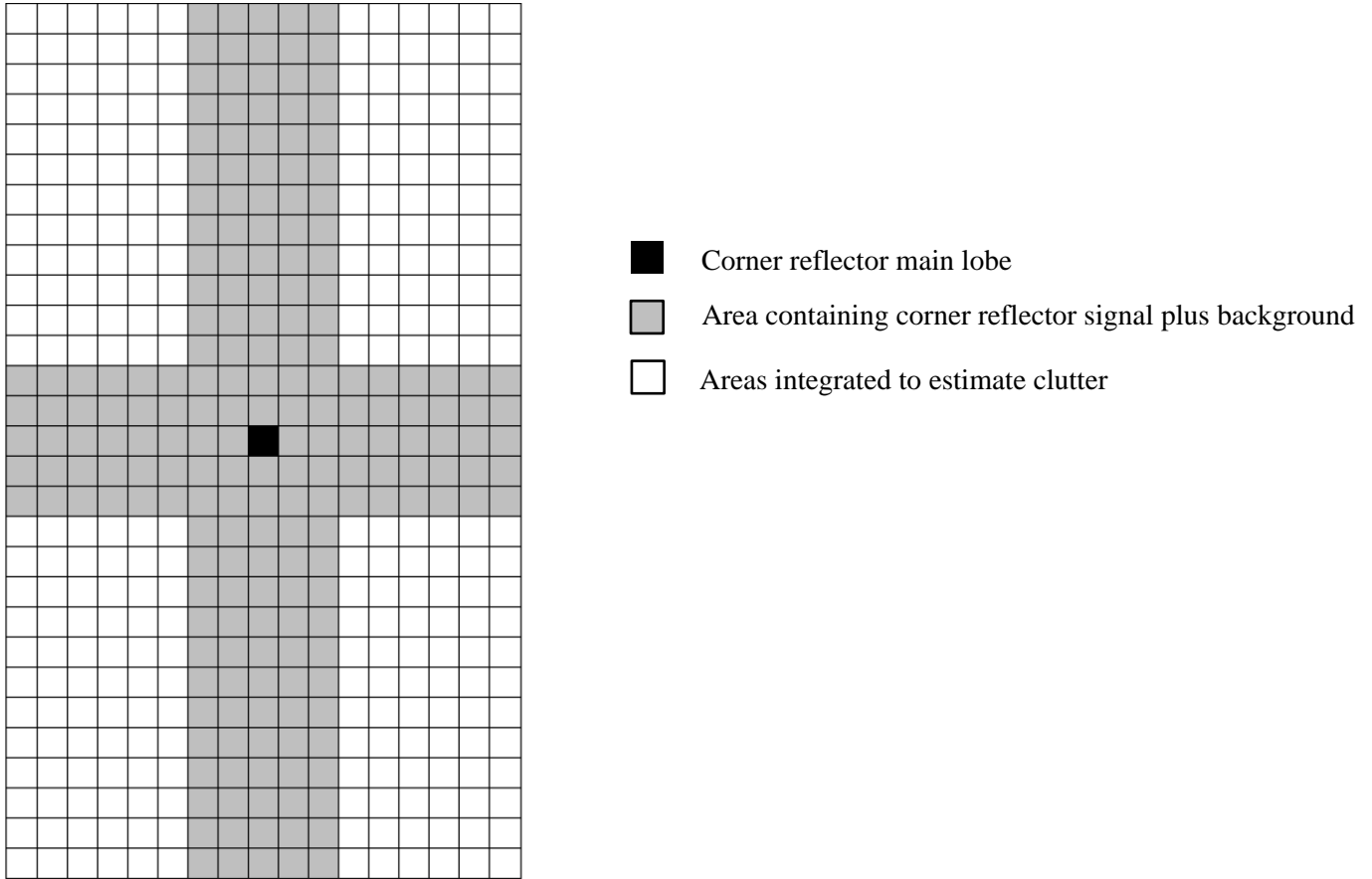


**Figure 5:** Definition of areas used during signal to clutter estimation in a SAR image. Modified from [13].

### 2.3 Geolocation accuracy

Following [18], which includes a modified form of earlier work by Stein [46] and Swerling [47], the theoretical lower limit for the *precision* (i.e. the standard deviation) with which the location of the main lobe peak may be identified in a single image SAR observation (in length units) is related to the SCR (N.B. expressed in linear units, not dB) as follows:

$$\sigma_{CR} = \frac{\sqrt{3}}{\pi\sqrt{2}} \cdot \frac{1}{\sqrt{SCR}} \cdot \rho_{r,a} \approx \frac{0.39}{\sqrt{SCR}} \cdot \rho_{r,a} \quad \text{Eq. 3}$$

where  $\rho_{r,a}$  refers to one of the range or azimuth resolutions.

For example, given a S-1 (C-band) IW SLC product having  $\rho_{r,a}$  values of 3 m (slant range) and 21.7 m (azimuth), a target having a linear (intensity ratio) SCR value of 31.6 (corresponding to 15 dB) will have a theoretical observation precision given by  $\sigma_{CR} \approx \frac{0.39}{\sqrt{31.6}} \cdot 3 \approx 0.21$  m in range, and  $\sigma_{CR} \approx \frac{0.39}{\sqrt{31.6}} \cdot 21.7 \approx 1.50$  m in azimuth.

The tables below provide theory-based estimates of the dependence of the Absolute Location Error (ALE) on corner reflector size and vice versa. They may be used in three different ways:

1. For a corner reflector of a given *size*, its theoretical contribution to *ALE precision* and *phase error* can be estimated as follows:

- Look up the RCS of the corner reflector (given by the CR size and radar wavelength) from **Table 3**.
- Look up the RCS of the clutter (given by the beta naught of the clutter and of the size of the resolution cell) from **Table 4**.
- Compute the SCR in dB by subtracting the clutter RCS from corner reflector RCS (RCS given in dBm<sup>2</sup>).
- Look up the resolution corresponding to a given TSX or S-1 SLC product in **Table 5**
- Look up the ALE precision error or phase error (given by the SCR and reference resolution) in **Table 6** or **Table 7**, respectively.

*Example: A 1.5 m reflector has RCS of 38.3 dBm<sup>2</sup> in C-Band (**Table 3**). In S-1 IW1 we expect a clutter of 16 dB, assuming a  $\beta_0$  of -8 dB (**Table 4**). The expected SCR is therefore 38.3 dB – 16 dB=22.3 dB.*

**Table 3** gives an ALE of ca. 0.6 m in azimuth and 0.1 m in range for S-1 IW1 resolution.

- For a given ALE requirement, a theoretically recommended size of the corner reflector can be estimated as follows:
  - Look up the resolution corresponding to a given TSX or S-1 SLC product in **Table 5**
  - Look up the required SCR from **Table 6** (in the column of the known resolution, find the row the required ALE occurs in, and find the corresponding SCR in the first column)
  - Look up RCS of the clutter (given by the beta nought of the clutter and of the size of the resolution cell) from **Table 4**
  - Compute the required RCS of the corner reflector in dB by adding the clutter RCS to the SCR in dB
  - Look up the CR size from **Table 3** (find the row containing the given RCS in the column of the known radar wavelength, and look up the CR size in the first column).

*Example: To locate a CR in a TSX Staring Spotlight mode ST300 (0.6 m range resolution) with 1 mm range accuracy, an SCR of 45 dB is required.*

*Assuming a  $\beta_0$  of -8 dB, the clutter is -10 dB at this high resolution (**Table 4**). Therefore a CR with a RCS of 35 dBm<sup>2</sup> is required, resulting in a size of 1 m (**Table 3**).*

- For a given phase error requirement, the theoretical corner reflector size can be estimated.
  - Look up the resolution corresponding to a given TSX or S-1 SLC product in **Table 5**
  - Look up required SCR in **Table 7** (find the row containing the required phase error in the column of the known resolution, and look up the SCR in the first column)
  - Look up the clutter RCS from **Table 4** (given by the beta nought of the clutter and of the size of the resolution cell)
  - Compute the required RCS of corner reflector in dB by adding clutter RCS to SCR in dB
  - Look up the CR size from **Table 3** (i.e. find the calculated RCS in the column corresponding to the known radar wavelength, and look up the CR size in the first column)

**Table 3:** Theoretical RCS [dBm<sup>2</sup>] of triangular trihedral corner reflectors ( $\sigma_{\text{triangle, peak}} = \frac{4\pi a^4}{3\lambda^2}$ )

Inner edge length [m] (a in <b>Figure 3b</b> )	RCS X band [dB] e.g. TerraSAR-X $\lambda=3.1$ cm	RCS C band [dB] e.g. Sentinel-1 $\lambda=5.6$ cm	RCS L band [dB] e.g. ALOS-2 $\lambda=24$ cm
0.5	24.35	19.22	6.58

0.7	30.20	25.06	12.42
1.0	36.39	31.26	18.62
1.5	43.44	38.30	25.66
2.0	48.43	43.30	30.66
2.5	52.31	47.17	34.53
3.0	55.48	50.34	37.70
4.0	60.48	55.34	42.70

**Table 4:** RCS [dBm<sup>2</sup>] of theoretical clutter ( $\sigma_{clutter} = \beta_0 \cdot (2\rho_a \cdot 2\rho_r)$ )

$\beta_0$ [dB]	TSX	TSX	TSX	TSX	TSX	S-1	S-1	TSX	S-1	S-1	TSX	S-1	S-1
	ST300	HS300	HS	SL	SM	Beam S1	Beam S6	SC	IW1	IW3	Wide SC	EW1	EW5
	0.6 m <sup>2</sup>	2.6 m <sup>2</sup>	5.3 m <sup>2</sup>	8.2 m <sup>2</sup>	16 m <sup>2</sup>	29 m <sup>2</sup>	71 m <sup>2</sup>	89 m <sup>2</sup>	240 m <sup>2</sup>	320 m <sup>2</sup>	530 m <sup>2</sup>	1400 m <sup>2</sup>	2500 m <sup>2</sup>
-2	-4	2	5	7	10	13	16	17	22	23	25	29	32
-4	-6	0	3	5	8	11	14	15	20	21	23	27	30
-6	-8	-2	1	3	6	9	12	13	18	19	21	25	28
-8	-10	-4	-1	1	4	7	10	11	16	17	19	23	26
-10	-12	-6	-3	-1	2	5	8	9	14	15	17	21	24
-12	-14	-8	-5	-3	0	3	6	7	12	13	15	19	22
-14	-16	-10	-7	-5	-2	1	4	5	10	11	13	17	20
-16	-18	-12	-9	-7	-4	-1	2	3	8	9	11	15	18
-18	-20	-14	-11	-9	-6	-3	0	1	6	7	9	13	16
-20	-22	-16	-13	-11	-8	-5	-2	-1	4	5	7	11	14
-22	-24	-18	-15	-13	-10	-7	-4	-3	2	3	5	9	12
-24	-26	-20	-17	-15	-12	-9	-6	-5	0	1	3	7	10

**Table 5:** 3 dB resolution  $\rho$  for different TerraSAR-X and Sentinel-1 SLC products

Sensor/ Mode	TSX	TSX	TSX	TSX	TSX	S-1	S-1	TSX	S-1	S-1	TSX	S-1	S-1
	ST300	HS300	HS	SL	SM	Beam S1	Beam S6	SC	IW1	IW3	Wide SC	EW1	EW5
Azimuth	0.24	1.1	1.1	1.7	3.3	4.3	4.9	18.5	22.5	22.6	40	43.7	44
Range	0.6	0.6	1.2	1.2	1.2	1.7	3.6	1.2	2.7	3.5	3.3	7.9	14.4

**Table 6:** Clutter contribution to ALE [m] ( $\sigma_{CR} = \frac{\sqrt{3}}{\pi\sqrt{2}} \cdot \frac{1}{\sqrt{SCR}} \cdot \rho_{r,a} \approx \frac{0.39}{\sqrt{SCR}} \cdot \rho_{r,a}$ )

SCR [dB]	Reference resolution [m]												
	0.2	0.6	0.8	1	1.5	2	2.5	5	8	15	20	30	45
10	0.0247	0.0740	0.0987	0.1233	0.1850	0.2467	0.3083	0.6166	0.9866	1.8499	2.4666	3.6999	5.5498
15	0.0139	0.0416	0.0555	0.0694	0.1040	0.1387	0.1734	0.3468	0.5548	1.0403	1.3871	2.0806	3.1209
20	0.0078	0.0234	0.0312	0.0390	0.0585	0.0780	0.0975	0.1950	0.3120	0.5850	0.7800	1.1700	1.7550
25	0.0044	0.0132	0.0175	0.0219	0.0329	0.0439	0.0548	0.1097	0.1755	0.3290	0.4386	0.6579	0.9869
30	0.0025	0.0074	0.0099	0.0123	0.0185	0.0247	0.0308	0.0617	0.0987	0.1850	0.2467	0.3700	0.5550
35	0.0014	0.0042	0.0055	0.0069	0.0104	0.0139	0.0173	0.0347	0.0555	0.1040	0.1387	0.2081	0.3121
40	0.0008	0.0023	0.0031	0.0039	0.0059	0.0078	0.0098	0.0195	0.0312	0.0585	0.0780	0.1170	0.1755
45	0.0004	0.0013	0.0018	0.0022	0.0033	0.0044	0.0055	0.0110	0.0175	0.0329	0.0439	0.0658	0.0987
50	0.0002	0.0007	0.0010	0.0012	0.0018	0.0025	0.0031	0.0062	0.0099	0.0185	0.0247	0.0370	0.0555
55	0.0001	0.0004	0.0006	0.0007	0.0010	0.0014	0.0017	0.0035	0.0055	0.0104	0.0139	0.0208	0.0312

**Table 7:** Clutter contribution to phase error [deg] ( $\sigma_{phase} = \frac{1}{\sqrt{2 \cdot SCR}} \cdot \rho_{r,a} \cdot \frac{180^\circ}{\pi rad}$ )

SCR [dB]	Reference resolution [m]												
	0.2	0.6	0.8	1	1.5	2	2.5	5	8	15	20	30	45
10	2.6	7.7	10.2	12.8	19.2	25.6	*	*	*	*	*	*	*
15	1.4	4.3	5.8	7.2	10.8	14.4	18.0	*	*	*	*	*	*
20	0.8	2.4	3.2	4.1	6.1	8.1	10.1	20.3	*	*	*	*	*
25	0.5	1.4	1.8	2.3	3.4	4.6	5.7	11.4	18.2	*	*	*	*
30	0.3	0.8	1.0	1.3	1.9	2.6	3.2	6.4	10.2	19.2	25.6	*	*
35	0.1	0.4	0.6	0.7	1.1	1.4	1.8	3.6	5.8	10.8	14.4	21.6	*
40	0.1	0.2	0.3	0.4	0.6	0.8	1.0	2.0	3.2	6.1	8.1	12.2	18.2
45	0.0	0.1	0.2	0.2	0.3	0.5	0.6	1.1	1.8	3.4	4.6	6.8	10.3
50	0.0	0.1	0.1	0.1	0.2	0.3	0.3	0.6	1.0	1.9	2.6	3.8	5.8
55	0.0	0.0	0.1	0.1	0.1	0.1	0.2	0.4	0.6	1.1	1.4	2.2	3.2

\*=not feasible for InSAR applications, as value exceeds 30 degrees

## 2.4 Placement and orientation

One of the factors influencing the precision attainable using a CR measurement in a SAR image is the SCR of the target. The theoretical details were discussed in section 2.3; comparisons with actual measured values are shown and discussed in Appendix A for interested readers. For a given reflector, mainly two factors influence the SCR of

its imaged impulse response: the clutter intensity near the CR and its orientation relative to the SAR viewing direction.

### 2.4.1 Reflector placement

Given a CR of known dimensions and other acquisition constraints, the simplest way to guarantee maximum SCR is to place the CR in a location of low clutter intensity (low backscatter from the surroundings). For practical planning purposes, this can most simply be achieved by studying potential test sites in existing SAR images of the type planned for the CR acquisitions (imaging mode, product type(s)). Large areas that appear dark in the SAR images are generally ideal (naturally, excluding shadows). One should keep in mind that to ensure a “clean” impulse response function (IRF) from the CR, no strong scatterers – or their sidelobes – should be visible within at least several samples in all directions from the planned CR location. This means that products with larger sample spacings (e.g. S-1 EW mode products) require proportionally larger low-clutter areas for ideal CR placement.

If more than one CR is to be deployed at the same site, their IRFs may interfere with each other if they are either too close together, or oriented such that their sidelobes overlap with the other’s main lobe. As a general rule, CRs deployed facing the same direction should be staggered such that their IRFs only minimally intersect (if at all), and be placed as far apart as possible. If they are oriented towards different orbits (ascending vs. descending), only one at a time will show a strong response in a given image, making it possible to place reflectors of opposing orientation relatively close together.

For CR campaigns intended for geometric calibration or validation – with measurements typically performed at the cm- or even mm-level – very high CR stability/structural support is required. In the case of concrete or asphalt test sites, the CRs can be weighed down to minimise the chance of them being moved in the presence of strong winds. If only test sites with softer ground (e.g. fields) are available, then especially for longer observation periods, it may be necessary to build more stable foundations for the CRs. This could include anything from steel rods mounted in bedrock to poured concrete foundations and/or pedestals or other supporting structures. Several examples of these types of installations are shown and discussed in sections 3.1 and 3.3.

Large concrete or asphalt surfaces without nearby structures are ideal, as they reflect the incoming radar pulses away from the sensor and therefore ensure minimal clutter intensity as well as a stable foundation. UZH has often deployed its CRs in military-owned enclosures (e.g. unused airport runways or taxiways) to minimise the possibility of them being moved or damaged. However, fields with short grass may also generate low enough backscatter to make high SCRs possible, depending on the SAR wavelength and imaging mode(s).

Placing CRs near metallic structures, especially when aligned with the azimuth (orbital path), also comes with the risk of generating bright artefacts that could interfere with the CR signal. Nearby, above-ground electrical power lines also pose a risk, as they are recorded as linear artefacts with orientation dependent intensity [8].

A final consideration during the CR placement (as well as its orientation) is the possibility of magnetic interference on the compass used for its horizontal orientation. If the potential location is near large metallic or electrical objects or devices, possible false compass readings might impair CR orientation. For example, CR locations near metal fences, cars, metallic structures and electrical power lines are potentially problematic, even without considering possible geometric or radiometric artefacts in the SAR images themselves. While no reliable general rule exists for determining whether interference will be significant for a given location, it is best in practice to take multiple compass readings from positions at varying distances from the reflector to check for unexpected variations.

### 2.4.2 Reflector orientation

As stated earlier, one reason that triangular trihedral CRs are often selected for use in geometric and radiometric SAR calibration is their relatively flat RCS response curve. Given a CR with a fixed orientation (the simplest case), it will usually need to be installed with an elevation angle corresponding to a “mean” value corresponding to two or more satellite tracks for a given orbital direction (ascending or descending). This is possible thanks to the relatively flat response of trihedrals, where the relative RCS only decreases by  $\sim 1$  dB at  $10^\circ$  off-boresight (see **Figure 4**).

When orienting a trihedral CR for a spaceborne mission, one should therefore:

(a) set its azimuth (horizontal) angle to the approximate scene heading of the orbital tracks in consideration. As a first approximation, the reflector will then be oriented towards  $\sim 90^\circ$  counter-clockwise relative to the satellite heading for a right-looking sensor, i.e. looking towards the sensor at its closest approach,

(b) set its elevation angle to the mean satellite elevation, considering the various acquisition tracks planned.

The CR azimuth and elevation angles are defined to apply to the CR boresight axis. As orientation measurements, (e.g. using a compass) are more readily made relative to the CR baseplate and its edges, it is important to define the orientation relative to the baseplate. Following the nomenclature in **Figure 4a**, the boresight axis for a trihedral CR corresponds to  $\psi \sim 35.3^\circ$  and  $\theta = 45^\circ$  [9]. This means that when using e.g. an electronic level for CR elevation measurement, the desired boresight elevation can be calculated as:

$$\text{CR baseplate elevation angle} = \text{CR boresight elevation angle} - 35.3^\circ \quad \text{Eq. 4}$$

In order to plan the CR orientation, knowledge of the satellite tracks and the corresponding local incident angles are needed. A useful web site that UZH has regularly used as a planning tool is [calsky.com](http://calsky.com). It permits the definition of a target location and the selection of a particular satellite. For most remote sensing satellites, the orbital elements are publicly available and can be accessed automatically by satellite tracking software. After setting some restrictions on the angles and time range, the satellite positions at the user-defined location are calculated for zero-Doppler with both the azimuth and elevation angles provided directly (most SAR data currently available is provided in zero-Doppler geometry; exceptions such as older ALOS PALSAR datasets may have small, non-zero Doppler centroids not exceeding  $\sim 1^\circ$  [35]). An example is shown in **Figure 6** for S-1A, for the *Dübendorf* site in Switzerland and two dates in March 2017. Only the CR (1) azimuthal (or aspect) angle, i.e. the geographic heading and (2) elevation angles are required for CR installation. They are returned by the [calsky.com](http://calsky.com) interface as the *az* and *h* values (highlighted yellow in **Figure 6**).

An electronic level may then be used to measure the desired elevation angle *h*, while a compass can be used to set the azimuth angle *az*. Details on these procedures are given in section 3.3.2.

Another commonly used open-source software package used for satellite acquisition planning is STK [1].

### Friday 24 March 2017

Time (24-hour clock)	Object (Link)	Event
18h15m25s	 Sentinel 1A (39634 2014-016-A) →Ground track →Star chart	Ascending Orbit <b>Culmination 18h15m25s</b> az:259.9° W h:52.9° incidence-angle:37.1° distance: 856.7km height above Earth: 702.2km elevation of Sun: +4° angular velocity: 0.52°/s Side-look 18h15m28s az:262.2° W h:52.8° Relative to Sat: Squint-angle: 90.0° (right) Offnadir: 33.0° Range:856.9km <b>0-Doppler</b> 18h15m31s az:264.9° W h:52.8° Relative to Sat: Squint-angle: 92.7° (right) Offnadir: 33.0° Range:857.8km TLE epoch: 17086.79581970

### Tuesday 28 March 2017

Time (24-hour clock)	Object (Link)	Event
7h34m53s	 Sentinel 1A (39634 2014-016-A) →Ground track →Star chart	Descending Orbit Side-look 7h34m50s az: 97.4° E h:50.6° Relative to Sat: Squint-angle: 90.0° (right) Offnadir: 34.8° Range:879.7km <b>0-Doppler</b> 7h34m52s az: 99.0° E h:50.6° Relative to Sat: Squint-angle: 91.6° (right) Offnadir: 34.8° Range:879.5km <b>Culmination 7h34m53s</b> az: 99.7° E h:50.6° incidence-angle:39.4° distance: 879.4km height above Earth: 702.3km elevation of Sun: +3° angular velocity: 0.47°/s TLE epoch: 17086.79581970

**Figure 6:** Extract of S-1A orientation calculations for the Swiss *Dübendorf* site at the end of March 2017, generated at <https://www.calsky.com>

## 3 CALIBRATION CAMPAIGN: PRACTICAL CONSIDERATIONS

### 3.1 Trihedral corner reflector design considerations

Trihedral CRs are commonly used for geometric SAR calibration campaigns for the reasons described in section 2.1. However, some practical aspects of the CR design are important to consider during planning and deployment.

As already stated in section 2.4.1, a very high degree of stability is required. This not only applies to the mounting surface itself (e.g. asphalt vs. grassy field), but also the inherent stability of the CR, which includes the base or fixture it is mounted on. Today it is possible to attain cm-level geometric accuracy (or better) using well-established survey methods in conjunction with C-band and X-band spaceborne SAR image products. The CR and its mount should therefore be stable enough to guarantee that no additional errors will be introduced by heavy winds, rain, snow and long-term exposure to the elements. If placed directly onto a hard surface, the CRs may be weighed down to prevent small movements during heavy winds; an example of this can be seen in **Figure 17**. Alternatively, the CR base may be bolted to another solid structure or foundation, either to raise it above the maximum snow level (**Figure 7**, **Figure 8**) or simply provide a solid foundation on otherwise softer ground (**Figure 9**). Ideally, it should also be possible to adjust the CR orientation (azimuth and elevation) accurately. This is especially true if its orientation needs to be changed periodically during a campaign (note that any change in azimuth or elevation also shifts the position of the CR vertex).

Different requirements and budget constraints may favour different CR designs, ranging from simple netting wire constructions assembled in the field to precision devices with well-defined planimetric and angular tolerances. A useful overview is also given in [15] (or a later publication by the same author [17]). Examples for precision devices are the 1.5 m CRs used by DLR for radiometric calibration and for geometric validation experiments in *Wettzell*. They were produced by Zarges, Germany and priced at ~10 k€ (shown for e.g. in **Figure 2** and **Figure 7**).

Many more details and additional CR design considerations can be found in [15], [16], [17] and [48].



**Figure 7:** A CR installed at the Finnish Geodetic Observatory *Metsähovi* in cooperation with DLR. A special tripod base was added to lift the CR above the maximum expected snow level.



**Figure 8:** Local weather conditions may require special arrangements. At GARS O’Higgins, Antarctic Peninsula, an additional 1 metre base raised the corner reflector above the winter snow level.



**Figure 9:** Where applicable, mounting on stable bedrock is a good alternative to a concrete foundation. Example from geodetic observatory *Metsähovi*, Finland. According to recommendations from the Finnish Geodetic Institute (FGI), the stand of the corner reflector was mounted on the 22mm rods. The holes drilled directly into the bedrock (~40 cm deep) were filled with rock epoxy glue manufactured by *Hilti*. (© images by FGI)

## 3.2 Surveying

### 3.2.1 Reference Frames

Geolocation accuracy estimates are based on comparisons between *imaged* CR positions and a *predicted* image location based on their *surveyed* coordinates. Such comparisons carry with them the assumption that the geodetic reference frames defined for the satellite positions (i.e. the orbit product) and the CR positions are identical. However, in a narrow sense, this is often not the case. Reference frames are conceptually specified by definitions and conventions, see for instance the global international terrestrial reference system (ITRS) [30] or the regional European Terrestrial Reference System (ETRS89). In practice they are established as frames (e.g. ITRF, ETRF) by computing sets of station coordinates including velocities, which may be updated when longer data series and newer methods enable improved realizations. Usually, the global ITRS (in its most recent ITRF realisation) is the basis for satellite position vector annotations when using on-board GNSS observations for precise orbit determination (POD). Provided that the ITRS methods and conventions have been maintained during the POD, these annotated satellite positions vectors define the ITRF for the epoch (acquisition date) of the SAR measurement. On the other hand, terrestrial GPS measurements of the CRs are generally provided in a local reference frame when carried out differentially. For example, in Switzerland the local frame is the Swiss Terrestrial Reference Frame CHTRF95, which is tied closely to the ETRS89 realisation (ETRF) for the epoch 1993.0 (i.e. midnight on the eve of January 1<sup>st</sup>, 1993). Both frames (CHTRF95 and ETRF) are coupled to the stable part of the Eurasian continental plate. ETRS89 is, in turn, defined at a particular date (or epoch) in 1989 to be identical to ITRS. In other words, since this 1989 date, the ITRF and ETRF frames have been slowly drifting apart due to decoupling of the ETRF from movement of the Eurasian plate. At the time of this writing, the cumulative shift in central Europe corresponds to ~70 cm horizontally. Thus, for geolocation estimation, one has to be aware that the CR coordinates stemming from the DGPS survey might need to be transformed into the ITRF used for annotation by the SAR processor. For the ETRF, one does this by using the ETRF to ITRF transformation (itself based on plate tectonic models), if possible even on a product-by-product basis. More information on this transformation can be found in [11].

In any case, the final reference coordinates of a CR need to be in the same global reference frame as the annotated satellite positions. In addition to this, one generally requires a reference epoch as well as the secular velocity (usually related to plate tectonics) to perform the best possible ALE assessment. Details on this are provided in [4].

### 3.2.2 DGPS survey

Given the high geometric accuracy and overall system stability of today's spaceborne SAR sensors, sensor calibration and validation experiments should include reference targets with positions known to ~cm accuracy. Assuming an inherently stable CR and its careful installation on a stable surface, the other major potential source of target position error is the surveyed target position itself. Measurement of the CR vertex position (corresponding to the brightest point in a SAR image) using differential GPS (DGPS) provides ~cm-level positioning if performed correctly. Using this method, a GPS receiver is used to measure the position of a reference survey point relative to a nearby GPS reference station, recorded over a period of 20-30 minutes to guarantee ~cm level accuracy. During post-processing of the data recorded by the receiver, the known position of the antenna at the reference station is converted to a survey point position via the baseline between the reference and receiver antennas. Additional corrections of the reference station position are made for the survey time, which should include e.g. atmospheric and tectonic corrections. These corrections are transferred to the survey point position during post-processing as well.

As it is not possible to place a GPS receiver antenna at the position of the CR vertex directly, a reference point position is surveyed instead. This can be a well-defined point on the ground over which the CR is to be mounted. For both the S-1A/B in-orbit commissioning phases, UZH deployed CRs at two sites in Switzerland, which had either asphalt or concrete surfaces. In **Figure 10**, the reference points for the Swiss *Dübendorf* and *Torny-le-Grand* sites are shown in (a) and (b), respectively. In *Dübendorf* (a), the reference point shown is an easily visible pebble embedded in the asphalt; in *Torny-le-Grand* (b), existing mounting bolts for machinery could be used directly. The orange markings (spray paint) shown in (a) help surveyors locate the reference pebble later if necessary, in case of later CR repositioning or if survey updates are needed. Regular survey updates are not recommended for short-term campaigns, as each new survey will introduce new position biases (albeit small ones) and complicate statistical analysis of the combined time series. However, because of reference frame drift (e.g. caused by errors in tectonic modelling), longer-term (or permanent) CR installations may benefit from repeated surveys, whether performed by

removing the CRs and surveying the reference points, or by indirect differential methods such as described in the next section.

Reference points are surveyed using a GPS receiver as shown in **Figure 11**. The GPS antenna is located above the reference point with a known vertical offset. A bubble level ensures vertical alignment, although in practice small deviations at the ~mm level are possible depending on the equipment used.

The distance to the GPS reference station is connected to the final position error; the nearer the receiver is to the reference station, the higher the achievable positioning accuracy. For the Swiss test sites, two permanent reference stations were used, both part of the Automated Global Navigation Satellite System Network of Switzerland (AGNES) network. The nearest AGNES station from the *Torny-le-Grand* site was ~5 km away (station code PAYE); for Dübendorf, the nearest station was ETH2, located ~11 km from the test site.

A DGPS survey generally needs to record data over a period of 15-30 minutes in order to achieve the desired ~cm level accuracy. The estimated precision of the measurement is often provided by the post-processing software, and it depends on many factors, but mainly the integration (survey) time and the particular arrangement of GPS satellites at the time of the survey. For the Swiss sites, a Trimble R7 GPS receiver was used (visible in **Figure 11a**). The precision reported by the software during post-processing (Trimble Business Office) was specified as ~1 cm (horizontal and vertical) error at each site, with an RMS error of ~1-2 mm in each case. While the exact method used by the commercial software to arrive at these estimates is not openly documented, the reports it generates (“baseline reports”) provide auxiliary information that may be helpful in judging the plausibility of the precision estimates.



(a)



(b)

**Figure 10:** Reference mark close-ups, with GPS measurement leg placement during survey (a) Reference mark at *Dübendorf*, an easily visible pebble. The orange markings were added to help find the reference mark later (b) Reference mark at *Torny-le-Grand*, where small metal plates had already been implanted in the concrete.



(a)



(b)

**Figure 11:** GPS survey in *Dübendorf* in April 2016 (a) DGPS survey with antenna aligned vertically over reference mark (b) Close-up of integrated bubble level indicating vertical alignment

### 3.2.3 Terrestrial Geodetic Survey

For long-term ALE monitoring aiming at ~1-2 centimetre geometric accuracy, the integration of terrestrial SAR calibration infrastructure (usually CRs) into an existing global geodetic network should be considered. Such integration typically begins with a terrestrial geodetic survey at ~mm level accuracy. Subsequent geodetic surveys of additional CRs may be made relative to the network, providing an alternate approach to DGPS surveys of individual reference points. The main requirements are a permanent geodetic survey network typically supported by a set of concrete piers (embedded pillars) with mounts for geodetic survey equipment, as well as transformation parameters connecting the local network to the global International Terrestrial Reference Frame (ITRF), obtained via a GNSS survey of the network. These requirements are met especially well by geodetic observatories that utilise two or more geodetic space observation techniques, because determining the offset between the results obtained using different geodetic techniques through on-site surveying is paramount for establishing the ITRF solution [33]. The secular displacement rates associated with the ITRF are based on the observations made at these stations and are computed as part of the ITRF solution [2]. Therefore, such geodetic stations are ideal places for installing SAR CRs, because global reference coordinates (as defined in section 3.2.1) can easily be established at the mm-level when co-locating SAR with the other geodetic techniques. Also, the station sites should carefully consider the local geological stability, with the aim of guaranteeing stable targets for spaceborne SAR ALE monitoring. Approximately 15 sites worldwide (the so-called core sites) are connected as part of the Global Geodetic Observing System (GGOS) [21]. They all provide at least three geodetic solutions which are accessible worldwide, but there is high demand for increasing this number to some 30 stations with good global distribution [31]. At the same time, these goals open the possibility of integrating terrestrial SAR calibration infrastructure in the future. The newly defined requirements for co-locating the geodetic installations are at a ~0.1mm level [31], supporting the goal of achieving SAR observation accuracies better than ~5 mm at the global scale.

The terrestrial survey typically involves a tachymeter (geodetic total station), geodetic survey prisms and tribrachs to precisely mount the instrumentation. This setup allows for both angular triangulation and electronic distance measurement (EDM). Three geodetic stations – *Wetzell* (Germany), *Metsähovi* (Finland), and the German Antarc-

tic Receiving Station (GARS) O'Higgins (Antarctica) – are already equipped with radar CRs facing both ascending and descending orbits [18][23] for which the global reference coordinates have been determined using terrestrial survey methods. In the case of *Wettzell*, two reflectors were integrated into the station network [36] as part of local-tie campaigns. This was done by inserting a specially constructed metal cube into the drainage opening of the trihedral CR to complete the vertex. By threading a plumb-line through a hole drilled diagonally into the cube (corner to corner), the vertical projection of the vertex could be determined on the ground. A stainless steel rod with a mount for a geodetic survey prism was embedded in concrete at this point (see **Figure 12**). Finally, the measurement of the vertical offset between the mounting point and the reflector vertex made it possible to determine the CR vertex in a survey (see **Figure 13a**). A quick measurement of the offset with a ruler provides a way to check if the orientation of the reflector has been changed. The same method for installing permanent prism mounts was also used for the two CRs located at GARS O'Higgins, but because these reflectors were considerably smaller – with 0.7m edge length compared to the 1.5m CRs at *Wettzell* – the mounting bolt for the survey prism could be attached directly to the base plate of the reflector mount (see **Figure 13c**).

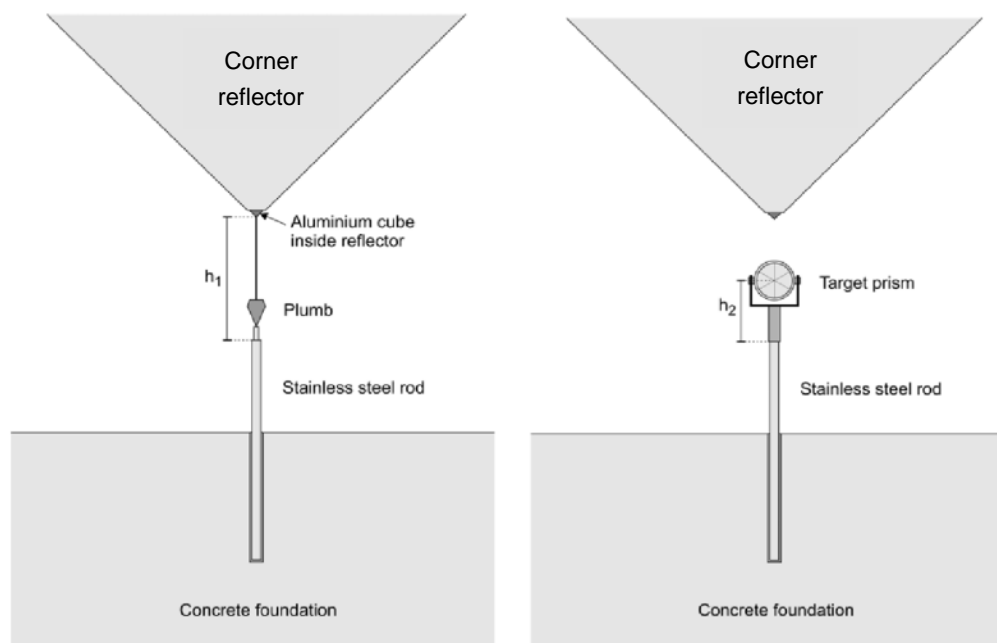


**Figure 12:** Permanent integration of a corner reflector into a geodetic survey network. A plumb-line is used to mark the vertical footprint of the reflector vertex, where a rod holding a survey prism is mounted in a concrete foundation. Taking into account the vertical offset allows direct survey via the target prism. Image credits to S. Mähler, T. Klügel, BKG.

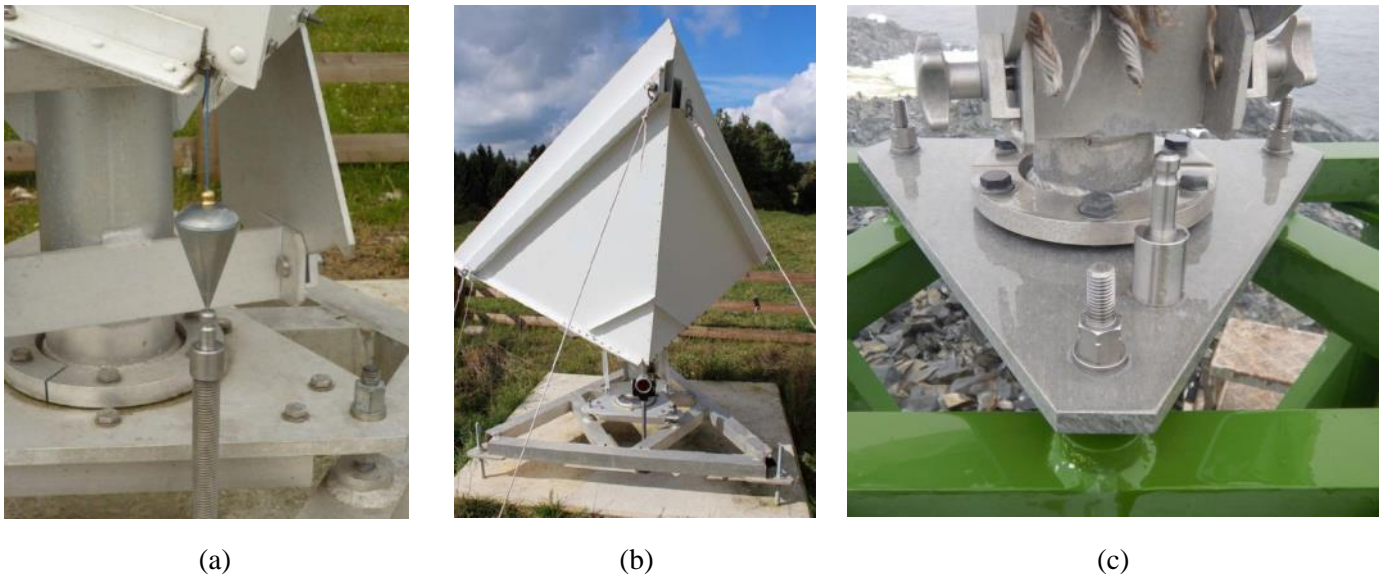


**Figure 13:** Examples of integration of corner reflectors into a local geodetic network (a) measurement of the vertical offset between a survey point and the 1.5 m CR vertex at geodetic observatory in *Wettzell*, Germany (b) installed reflector in *Wettzell* (c) 0.7 m CR installed in Antarctica. Image credits to S. Mähler and T. Klügel, BKG.

The method described is of course only meaningful if the orientation of the reflector is intended to remain fixed with a certain orientation, e.g. towards only ascending or only descending satellite passes. In the example of *Wettzell*, the survey was performed repeatedly from several piers by measuring full sets of angles and distances to other piers equipped with survey prisms, as well as to the survey prisms marking the two reflectors. The precision of the local coordinates computed from the measurements by least squares adjustment was better than  $\sim 1$  mm. The same holds true for the survey of the GARS O'Higgins reflectors, for which the estimated precision of the locally computed coordinates was reported as 1 mm. Given that the uncertainty of the local-to-global transformation parameters was typically  $\sim 2$ -3 mm [36] or better (for more recent results see for instance [24]), the current requirements regarding SAR can be met.

Without the installation of a prism mount, a terrestrial survey is still possible by performing angle measurements of the vertex itself. If the angles are measured from at least two survey piers, the coordinates of the vertex can be derived by triangulation. To improve the visual perception of the vertex during the survey, a brightly coloured corner cube could be placed inside the reflector. A computational approach can also be used to verify a direct angular survey of the reflector vertex, which is possible if one additionally surveys the tips of the reflector, e.g. the three tips of a trihedral reflector. The actual vertex is then calculated from the known reflector geometry using the tip coordinates from the survey to define the reflector in three-dimensional space.

At *Wettzell*, both angular methods were compared to the direct approach using the survey prism. The three sets of reference coordinates were found to be consistent to within  $\sim 2$ -3 mm, but regarding the estimated precision, the direct method is superior because of the additional EDM observations. Measuring the CR vertex by angular triangulation was also used to integrate the reflector at *Metsähovi* station. The precision of the survey result was reported to be better than 5 mm, which is consistent with experience at *Wettzell*.

The installation of SAR reflectors at geodetic observatories has many benefits when it comes to ALE monitoring of spaceborne SAR sensors. The observatories offer long-term stability and the chance to integrate SAR-based measurements into local station networks for the determination of global coordinates. They also provide all the data needed to perform the corrections required for ALE analysis of SAR image products. On-site meteorological sensors continuously log the state of the atmosphere (pressure, temperature, humidity, wind speed) and the permanently operated GNSS receivers can be used to determine the atmospheric path delays [33]. More details on these procedures are provided in the Site Survey Protocol Definition, see [4].

For a GPS reference station that does *not* provide the meteorological data needed for signal path delay correction, the minimum parameter set needed for SAR geolocation analyses is listed in the reference station protocol sheet described in the next section (3.2.4).

### 3.2.4 Survey protocol sheets

A DGPS survey of a SAR CR to be used for product ALE monitoring results should be connected to a reference station description. Together, the survey and reference station descriptions provide the inputs required for accurate ALE estimation in SAR image products.

UZH defined a pair of protocol sheets, shown in **Figure 14**, that capture the most important quantities connected to a DGPS survey in Switzerland. These sheets may be adapted for surveys anywhere in the world, and are designed to summarise the “output” of a DGPS point target survey.

At the top of **Figure 14** is the *point target survey protocol sheet*. It describes all relevant aspects of the target(s) itself; in this example, the targets are four trihedral CRs deployed at two sites in Switzerland. In addition to providing a general description of the target parameters (e.g. name, type, side length), the surveyed coordinates are first provided in the native (local) reference frame (e.g. CH1903+ LV95 in Switzerland). The coordinates are then listed in global Cartesian coordinates (conversion performed after the survey itself), which are usually the most useful, as they can be compared directly to the coordinates provided by most spaceborne SAR systems. Some parameters related to the survey process itself are provided next, e.g. the date/time and total integration time, as well as the precision estimates provided by the GPS software. Next, a more detailed description of the target(s) is given, with a section for active transponders provided as well. In particular, the local magnetic deviation from geographic north (called the magnetic declination) is an often neglected parameter that may be more or less relevant for CR azimuthal orientation using a compass. Comment areas are possible for the target columns, as well as for the individual descriptor fields.

The lower half of **Figure 14** is the *reference station protocol sheet*, which describes the most important parameters describing the DGPS reference station connected to the survey. Generally, such a station provides an accurate estimate of its position in a given geodetic reference frame(s), valid at a given epoch (date). Many stations will also provide estimates of their velocity within the ITRF, which is mainly due to the relative drift of tectonic plates. Both the drift rate and the validity date (reference epoch) are needed in order to obtain a valid ITRF position for a target imaged by a SAR system at a (usually later) date and time. The last section in the station protocol sheet is optional but potentially useful for later interpretation. It lists a station position calculated using the provided quantities for a given hypothetical “reference epoch” in the future, providing the basis for plausibility checking.

More detail on the use of the parameters described in these sheets for product ALE monitoring is provided in [4].

Point Target Survey Protocol						Comment(s)
Point target overview	Reference Point Name	UZH_TORNY_N	UZH_TORNY_S	UZH_DUEB_N	UZH_DUEB_S	N/S = north or south CR
	Reference Point Type	Trihedral corner reflector	Trihedral corner reflector	Trihedral corner reflector	Trihedral corner reflector	
	Corner reflector edge length [m]	1.50	1.50	1.20	1.00	
	Associated DGPS reference station name	PAYE	PAYE	ETH2	ETH2	Described on reference station sheets
	GPS hardware used for survey	Trimble R7 receiver	Trimble R7 receiver	Trimble R7 receiver	Trimble R7 receiver	
Point target position local cartographic frame	DGPS cartographic reference frame	CH1903+ (LV95)	CH1903+ (LV95)	CH1903+ (LV95)	CH1903+ (LV95)	Derived from CHTRS95 Swiss reference frame
	Easting [m]	2563138.048	2563155.728	2691784.894	2691769.747	Surveyed coordinates provided by GPS software; the height is adjusted to include vertical offset of CR vertex from survey point. Description of reference system: <a href="http://www.swisstopo.admin.ch/internet/swisstopo/en/home/topics/survey/sys/refsys/switzerland.html">http://www.swisstopo.admin.ch/internet/swisstopo/en/home/topics/survey/sys/refsys/switzerland.html</a>
	Northing [m]	1180044.896	1180017.009	1250201.460	1250151.606	
Height above ellipsoid [m]	729.981	728.989	443.654	443.766		
Point target position converted to global Cartesian coordinates	X [m]	4344625.707	4344642.962	4276445.745	4276484.320	Datum shift (local to global) defined in section 1.4 of "Formulas and constants for the calculation of the Swiss conformal cylindrical projection and for the transformation between coordinate systems", 2008, available at swisstopo.ch
	Y [m]	530069.035	530089.126	650909.334	650899.104	
	Z [m]	4624900.452	4624880.702	4672057.834	4672024.332	
Survey description	Survey date	22.04.2016	22.04.2016	27.04.2016	27.04.2016	In baseline report generated by Trimble Business Center
	Survey time [UTC]	11:57:00	12:33:00	07:46:00	07:14:00	In baseline report generated by Trimble Business Center
	Type of measurement (static / RTK / stop-and-go)	static	static	static	static	
	Horizontal precision [m]	0.007	0.007	0.0099	0.0134	In baseline report generated by Trimble Business Center
	Vertical precision [m]	0.0105	0.0121	0.0124	0.0131	In baseline report generated by Trimble Business Center
	Survey duration [minutes]	22	24.5	20.75	20	In baseline report generated by Trimble Business Center
	Max. PDOP	1.856	1.393	1.705	1.496	In baseline report generated by Trimble Business Center
Corner reflector description	Corner reflector type	Trihedral	Trihedral	Trihedral	Trihedral	
	Side length [m]	1.50	1.50	1.20	1.00	
	Peak RCS [dBm2]	38.4	38.4	34.5	31.3	S1 wavelength defined on sheet "Lists"
	Azimuth [°] - measured	97.2	266.7	265.3	94.7	As measured by magnetic compass
	Site magnetic declination [°]	2.3	2.3	2.3	2.3	Deviation of magnetic north from geographic north, e.g. <a href="http://www.magnetic-declination.com">http://www.magnetic-declination.com</a> ; positive value means eastwards deviation
	Azimuth [°] - geographic	99.5	269.0	267.6	97.0	Compass angle + magnetic declination = geographic angle
	Elevation [°]	53.6	50.0	63.1	60.7	Bore-sight (not base-plate)
	Validity start date	22.04.2016	22.04.2016	27.04.2016	25.05.2016	UZH_DUEB_S was rotated to face DSC orbit on 25.05.2016
	Validity stop date	31.12.2016	31.12.2016	31.12.2016	31.12.2016	
	Transponder description	Time delay [ms]	0.00	0.00	0.00	0.00
	Transmit polarisation [H, V, Linear 45deg]					
Comment(s)	2 cm drainage hole	2 cm drainage hole	0.5 cm drainage hole	0.5 cm drainage hole		

Reference Station Protocol				Comment(s)
	DGPS reference station name	PAYE (Payerne, near Torny-le-Grand)		
	ITRS realisation	ITRF2008		From sheet <a href="http://www.swisstopo.admin.ch/swisstopo/geodesy/pnac/restxt/multi_av_crd.txt">http://www.swisstopo.admin.ch/swisstopo/geodesy/pnac/restxt/multi_av_crd.txt</a> , which specifies "LOCAL GEODETIC DATUM: IGB08", which is equivalent to ITRF2008.
	National reference frame	CHTRF95		
	Reference epoch (validity date)	07.03.2006		Provided by swisstopo (file multi_ah_crd.txt, generated 2016.05.16)
	Reference citing connection between local system & ITRS	Schneider D. et al. Aufbau der neuen Landesvermessung der Schweiz 'LV95' Teil 3: Terrestrische Bezugssysteme und Bezugsrahmen Federal Office of Topography, Switzerland, 2002		
ITRF Cartesian coordinates	X [m]	4341234.776		Provided by swisstopo (file multi_ah_crd.txt, generated 2016.05.16); station "PAYE D", i.e. PAYE + the largest letter = newest measurement
	Y [m]	528725.681		
	Z [m]	4627897.037		
Station velocity within ITRS (due to plate tectonics)	dX [m/year]	-0.01414		Provided by swisstopo (file multi_ah_vel.txt, generated 2016.05.16); station "PAYE D", i.e. PAYE + the largest letter = newest measurement
	dY [m/year]	0.01851		
	dZ [m/year]	0.01037		
ITRF Cartesian (extrapolated to new epoch using station velocity)	New epoch	01.06.2016		Future epoch for extrapolated positions (New epoch - Reference epoch)
	Dt [years]	10.235674		
	X [m]	4341234.631		Calculated as reference position + (station velocity * time difference between new and reference epochs)
	Y [m]	528725.870		
Z [m]	4627897.143			

**Figure 14:** Complete survey protocol for accurate geolocation estimation: the first sheet (top) describes the survey of the reference target (the CR vertex position), the second (at the bottom) describes the associated GPS reference station in global ITRF Cartesian coordinates.

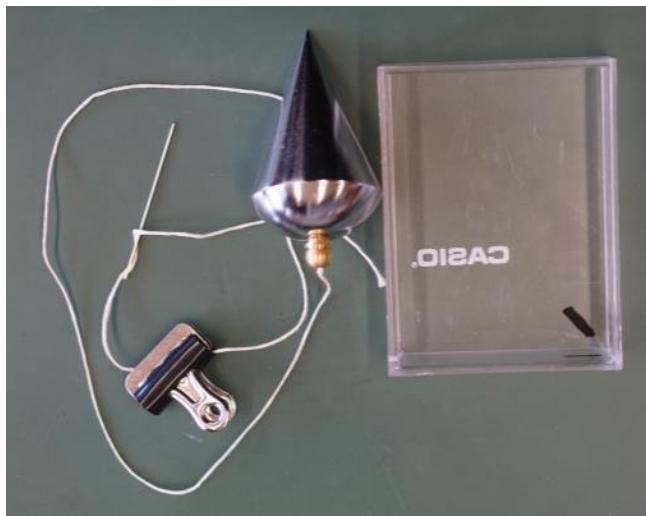
### 3.3 Corner reflector installation

Some initial considerations on CR placement and orientation were provided in section 2.4. These mainly considered theoretical and the most important *planning* aspects into account. This section provides further details on the positioning and orientation of a trihedral CR in the field, once the location and required orientation have been es-

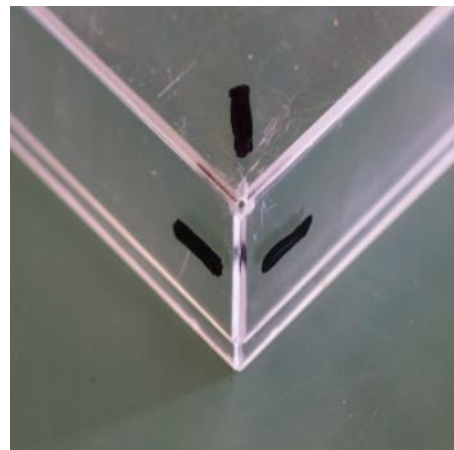
tablished. The advice is based mainly on experienced gained by UZH over many years of calibration/validation campaign experience connected to spaceborne SAR instruments.

### 3.3.1 Equipment and materials

At UZH, a collection of relatively inexpensive tools and techniques have been collected or designed, permitting simple positioning and orientation of a trihedral CR with high enough accuracy for SAR product geolocation monitoring. The tools are shown in **Figure 15**. They include (a) a weighted plumb line with pointed tip, (b) a hand-made corner cube for temporarily replacing a drilled-out vertex, (c) a flat-head screwdriver to be used as a simple lever, (d) an electronic level, (e) a magnetic compass with flat edges and an adjustable dial, (f) a tape measure suitable for accurate measurements beginning at ground level. Their use is described in the following section.



(a)



(b)



(c)



(d)



(e)



(f)

**Figure 15:** Equipment used for accurate CR placement and orientation (a) hand-made corner box for placement into the vertex drainage hole, with weighted plumb line, needle, thread and spring clip; used for precise orientation of the CR vertex over a reference mark (b) Small hole drilled into the corner of the box (c) flathead screwdriver used as a lever to nudge the CR base at mm scale (d) electronic level (e) compass with straight edges that can be aligned with the CR baseplate front-facing edge (f) metal ruler or tape measure for measuring the vertical offset between the CR vertex and the survey mark

### 3.3.2 Corner reflector placement and orientation for time-limited campaigns

Close alignment between CR axes and the SAR sensor is generally recommended to optimise the recorded signal backscatter. However, for CR campaigns dedicated to SAR product *geometric* quality monitoring, it is worth remembering that extremely precise orientation is *not critical*, as the RCS drops off quite slowly from the boresight axis, with  $\sim 1$  dB of reduction at  $10^\circ$  off-boresight. This is especially important when acquisitions from several orbits (i.e. different incident angles) are planned. In such cases, a reasonable orientation goal for such CRs is  $< 10^\circ$  overall, as the intensity of the imaged reflector will not be much reduced. At the same time, the misalignment should be kept to a minimum; with better alignment comes higher SCR, and in turn, slightly improved geolocation precision (as given by the measurements of the CR peak in the SAR images). Extremely accurate CR orientation (i.e. better than  $\sim 1^\circ$ ) has a higher priority if the CRs are to be used for *radiometric* quality monitoring (beyond the scope of this document).

A CR's azimuthal (horizontal) orientation can be measured with an accuracy of  $\sim 1$ - $2^\circ$  using a compass (**Figure 15e**), typically aligned with the front baseplate of the CR as shown in **Figure 16a**. Care must be taken to adjust the required angle by  $90^\circ$ , depending on which side of the compass is oriented flush against the baseplate edge. Also, the compass inner edge should be rotated slightly upwards to make it roughly level, as the CR baseplate will generally be tilted upwards.

If a magnetic compass is used to determine the CR's azimuthal angle, one should be aware of the location *magnetic declination*, i.e. the difference between geographic and magnetic north. The approximate magnetic declination for a user-selected site can be determined e.g. at <http://www.magnetic-declination.com>. In Switzerland, the declination was  $\sim 2.3^\circ$  in 2017. In order to maximise CR RCS, the declination should be taken into account when using a compass to orient the CR. In the example of Switzerland, a positive declination of  $2.3^\circ$  means that a *desired* geographic azimuthal angle of e.g.  $90^\circ$  (geographic east) would correspond to a compass heading of  $87.7^\circ$ . Failing to make this adjustment would cause a  $\sim 0.2$  dBm<sup>2</sup> RCS reduction in this example – not a large reduction, but easily avoidable.

There may be additional magnetic deviation coming from the CR installation itself, especially if ferrous materials were used to construct the CR, or in the presence of nearby ferrous objects (potentially even underground, e.g. pipes). We suggest checking this by aiming the compass towards the vertical edge of the CR from a distance, which is also described in [15].

The CR elevation may be set using an electronic level (**Figure 15d**), as shown in **Figure 16b**, with one end at the CR vertex. Its axis should be perpendicular to the front of the baseplate. Note that the baseplate slope is  $35.3^\circ$  below the boresight axis (Eq. 4).

Weather protection or drainage holes are generally required to prevent rainwater from regularly filling up the CR (which dramatically decreases its RCS). A 1.5 cm drainage hole is shown in **Figure 16c**; **Figure 18a-b** show rainwater accumulation caused by blocked 0.5 cm drainage holes. UZH has limited experience with single- and multiple-hole drainage implementations. Based on our experience, we recommend a single, large hole in the vertex as opposed to several small holes, as the large hole is less likely to become clogged with small objects such as leaves, nuts, pebbles, etc. The removal of the physical vertex to make a drainage hole does not in any way affect the position of the peak intensity in a SAR image, and the RCS reduction is negligible. However, the drainage hole converts the vertex position into a “virtual” space. As the vertex position nevertheless needs to be precisely determined (surveyed), locating it presents a minor challenge. For the survey, the vertex needs to be aligned vertically over the reference survey point on the ground, and its vertical offset from the survey point measured. A simple and accurate way to “regain” the actual vertex for survey purposes is to buy or construct a “corner cube”, previously mentioned in section 3.2.3. A simple version based on a solid plastic box with a sharp corner was constructed at UZH, shown in **Figure 15b**. A narrow hole was drilled through the corner for threading the plumb line. The plumb line itself is threaded through the hole using a sewing needle. Once the plumb weight is hanging just over the ground, the line is clamped in place using a metal clip, as shown in **Figure 16d**. A view of the suspended plumb line from outside the CR vertex is shown in **Figure 16e**, with the weighted tip as close to the ground as possible without touching it.

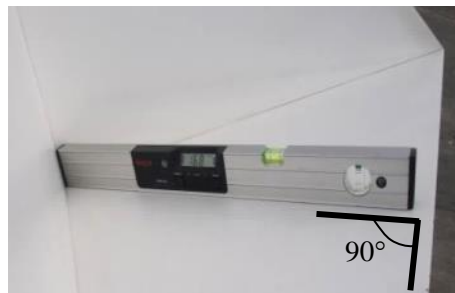
Next, the CR vertex (represented by the corner cube vertex) is placed over the survey point on the ground. UZH uses a flat-head screwdriver as a lever underneath the CR base to carefully nudge the CR into the correct position. Without such a lever (e.g. simply pushing the CR by hand), the required mm-level shift is difficult to achieve, as the CR is heavy and the friction tends to make smooth horizontal adjustments difficult.

Once vertical alignment has been achieved, the plumb line may be removed, and a tape measure (such as in **Figure 15f**) may be used to measure the vertical offset between the survey point and the true vertex (i.e. the corner cube vertex protruding from the drainage hole). This offset needs to be applied to the surveyed GPS position in local map coordinates (i.e. Easting/Northing/height) before the final transformation of the surveyed position into global Cartesian or geographic coordinates.

Finally, CRs should be weighed down if possible if they are not permanently installed, to prevent them from shifting slightly in windy conditions. Care should be taken to avoid aligning the straight edges of the weights perpendicular to the boresight direction; this minimises the chances of additional double-bounce reflections potentially falsifying the imaged position of the CR vertex. Two CRs are shown after being surveyed and weighed down at the Swiss site *Torny-le-Grand* in **Figure 17**, in preparation for S-1B calibration and validation.



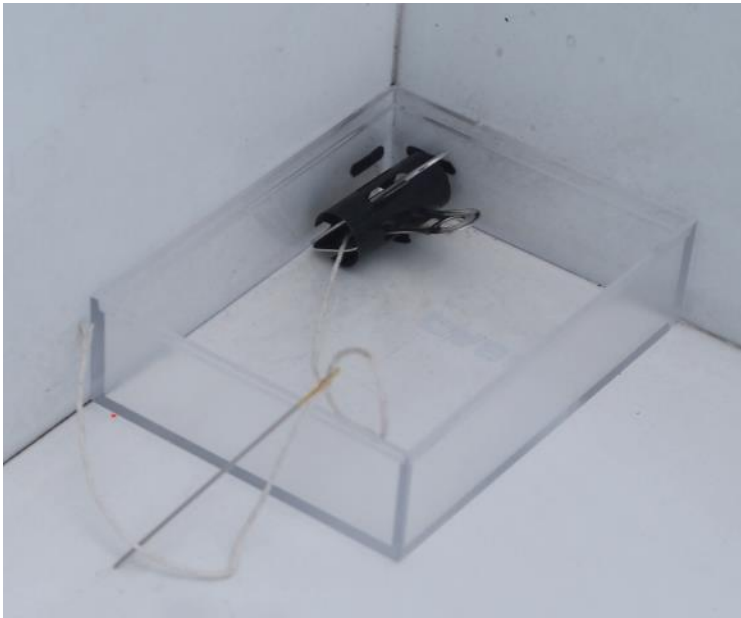
(a)



(b)



(c)



(d)



(e)

**Figure 16:** CR orientation and alignment of the vertex over the reference mark (a) using a compass to align the CR azimuth angle (b) using an electronic level to set the baseplate elevation (c) 2 cm drainage hole at vertex of a 1.5 m reflector (d) threaded corner box in the CR vertex, with clip holding the plumb line (e) plumb line vertically aligned over the survey mark



(a)



(b)



(c)

**Figure 17:** Installed and surveyed reflectors with each vertex aligned vertically over the reference mark, and the boresight axes oriented towards the expected satellite overpass (a) *Torny-le-Grand* 1.5 m (b) *Dübendorf* 1.0 m (c) *Torny-le-Grand* 1.5 m CR pair, oriented towards S-1's ascending and descending orbits.

### 3.3.3 Corner reflector weather protection

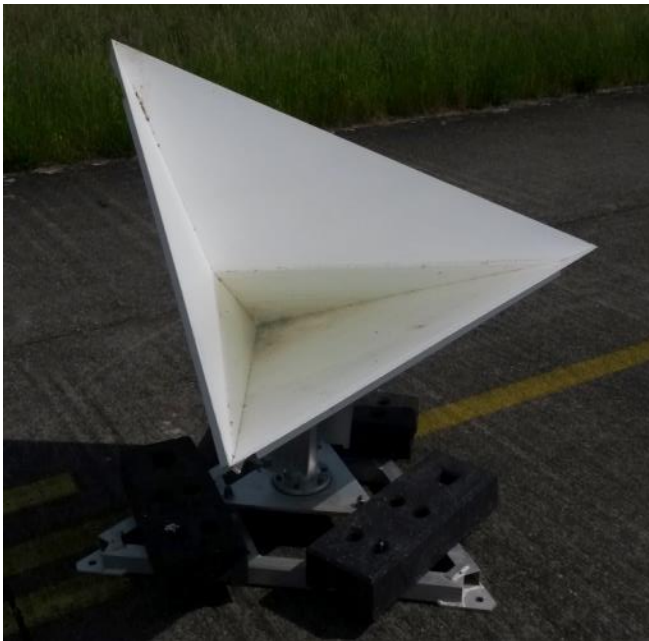
Corner reflectors are passive devices without any electrical components. In principle, they can be installed at any exposed, outdoor location on stable surfaces, or surfaces able to hold reflector mounts. Rainfall, however, poses a major problem for an unsupervised reflector installation, as there is a high risk that its drainage hole could get blocked by leaves or debris deposited by wind or birds, or by bird droppings (at some sites, birds enjoy the view from a perch on the tips of CRs, and may even attempt to build a nest in the CR). In such cases, the reflector may fill up with water during the next rainfall and its response will become severely damped, reducing the SCR to an insufficient level while decreasing the symmetry of the imaged response at the same time. In the winter, RCS-reducing snowfall is even more critical, as it will almost always accumulate within the reflector whether there is a drainage hole or not. Practical examples of SCR reduction due to rain and snow are discussed in section 4.

In the literature, several methods for mitigating these problems have been reported. In [15] and [32], perforated designs relying on meshed plates were discussed, which should offer improved self-cleaning ability and thus less chance of flooding during rainfall. Limitations were found in the process of punching the perforation as it affected the stability and planarity of the corner geometry when done for reflectors with larger than 1.5 m side lengths [15]. Moreover, removing material from the corner surfaces reduces its RCS by  $\sim 0.2$  dB for C-band and  $\sim 0.6$  dB for X-band. After evaluating the practical experience using the hole-punched prototypes, the authors of [15] and [32] decided not to pursue these designs further as the doubling in manufacturing costs and the problems with surface distortion due to the punching process outweighed the improvement in flooding mitigation.

A different strategy is to cover the reflector with a canvas or plates that are transparent to microwave signals, and which provide protection against rain and snow. The successful use of such coverings was reported by the Northern Research Institute (NORUT) for permanent installations of several trihedral CRs in northern Norway [25]. These reflectors were protected by PVC plastic canvas while the smaller reflectors were covered by plexiglass shields (see **Figure 19**). The coverings were installed in 2010 and the authors reported reliable SAR measurements for their reflectors even during the winter [26]. In the case of canvas covers, wind-induced vibration tended to remove thin snow layers that had accumulated [25]. The rigid plexiglass shields also accumulated some snow; in this case, enough sunshine was needed to warm them and initiate the self-cleaning.

Practical experience in dealing with snow was also gathered with the DLR/TUM CR installations at GARS O'Higgins, Antarctica. During the first year, the reflectors were operated without protective coverings, which resulted not only in a loss of sufficient backscatter for several acquisitions (see **Figure 24** and the discussion in section 4.2) - it also made the maintenance of the CRs much more cumbersome. During the stormy conditions usually accompanying the snowfalls, maintenance was, of course, impossible as it would pose an unacceptable risk to the on-site personnel. Thus, an experiment with Gore-Tex canvas (which is also used to protect the GARS O'Higgins communication antenna) was initiated in June 2014. Covering the reflectors with this canvas had no significant impact on the RCS, and therefore the coverage has been kept since (see **Figure 19c**). Maintenance is still performed on occasion, as thin layers of snow can have a small effect on the SCR, as it was already reported for the reflector installations at Norway. Nevertheless, the effort in cleaning the reflectors has been greatly reduced and only a very small number of observations had to be eliminated from DLR/TUM's systematic geometric observations after the covering was installed (see **Figure 24**). Overall, protective reflector coverage has proven to be an effective way to improve the all-weather capabilities and should be considered for unsupervised installations in remote areas with harsh environmental conditions.

In addition to the reflector shielding, the reflector mounts also have to be taken into account. As can be seen in the images in **Figure 19**, elevated reflector mounts are of great importance when reflectors are to be installed in regions with chances of heavy snowfall. Such mounts prevent the reflectors from becoming buried in snow and have to be designed according to the expected snow heights. The environmental conditions at the installation site have to be considered as well. For instance, at GARS O'Higgins the stands had an elevation of 1 m and were designed to withstand the strong winds occurring at this site.



(a)



(b)



(c)

**Figure 18:** Weather-related SCR reduction at Swiss test sites. (a) Water-filled corner reflector at UZH *Dübendorf* site before cleaning on 2016.05.25 (b) at *Dübendorf* during CR drainage on 2016.11.14 (c) at *Torny-le-Grand* on 2017.01.19 after a period of snowfall. Note that (a) and (b) are the same reflector, but the weighting blocks were moved on 2016.05.25 to reduce the possibility of interference from multiple-bounce effects.



(a)



(b)



(c)

**Figure 19:** Trihedral corner reflectors with different types of coverage for weather protection. (a) and (b) show covered reflectors employed by NORUT in Norway using PVC plastic canvas and plexiglass reported to be transparent to radar signals; images from [25], (c) shows a protected reflector at GARS O’Higgins station using a high-frequency transparent Gore-Tex canvas; image by DLR-DFD.

### 3.3.4 Protection against animals and vandalism

Corner reflectors often attract the interest of animals, which have been observed e.g. scratching their fur on the corners. In one case, a CR installed by DLR for landslide monitoring was destroyed by animals, most likely a cow. The CR in *Wetzell* is enclosed by a wooden fence to keep away sheep grazing in the surrounding fields (**Figure 20**).



**Figure 20:** Wooden fence in *Wetzell* to keep grazing sheep from the CR

In urban areas, animal-related problems may become unimportant, but the risk of vandalism or theft increases. If possible, CR sites that are not easily accessible to people or animals are preferred. This could include isolated regions outside of urban areas that are not easily accessible (possibly complicating the CR transport and installation), protected, enclosed areas such as military enclosures (preferred by UZH, but requiring special permission), or otherwise sites outside of urban areas that are not difficult to access, but with protection from farm animals, deer, etc. as needed (such as is depicted in **Figure 20**).

### 3.3.5 Field protocol sheet

When performing a DGPS survey of a newly installed CR, a “log sheet” for use in the field is strongly recommended. At UZH, one log sheet is prepared in advance for each CR, with the known information already filled in. An example of such a sheet, before use in the field, is shown in **Figure 21**. Experience has shown these log sheets to be useful when questions arise in connection with the CR or site. The information recorded by UZH includes at least:

- the name of the site and/or reflector
- the survey/installation date
- the name of the person responsible for the survey (esp. when more than one person is involved)
- the type and size of reflector
- the CR orientation (azimuthal and elevation angles)
- the elevation of the CR vertex above the survey point; if not directly above it, then its horizontal offset in the east/north directions
- the *approximate* CR location in global geographic coordinates (e.g. using Google Maps, smartphone GPS, etc. as a coarse reference)
- important GPS antenna parameters (GPS reference station, height of antenna phase center)
- comments related to the weather conditions during the survey or other aspects of the site/installation with potential relevance during data analysis

Sentinel 1B 2016 GPS measurement protocol			
<b>Site Name: Torny-le-Grand</b>		<b>Date: 21.04.2016</b>	
<b>Site ID: Torny_NE / Torny_SE</b>		<b>Operator(s): A. Schubert</b>	
<b>Site No.:</b>			
<b>Approximate Coordinates</b>			
Longitude [°]: 6.9562 E			
Latitude [°]: 46.7704 N			
Height (ellip) [m]: 731			
<b>Trimble System Parameters:</b>			
Local start time:		Antenna height: 1.80m	
Local stop time:		Measured to: top of notch <input type="checkbox"/>	
Reference ID: PAYE		phase centre <input type="checkbox"/>	
<b>WGS84 Coordinates:</b>			
Longitude [°]:	E	Input <input type="checkbox"/>	Calculated <input type="checkbox"/>
Latitude [°]:	N	Y	
Height (ellip) [m]:		Z	
<b>Corner Reflector</b>			
Inner edge length: 1.5m		Trihedral <input type="checkbox"/> Cube <input type="checkbox"/>	
<b>Offset from reference point:</b>		<b>Orientation :</b>	
ΔH [m]:		Azimuth =	
ΔN [m]:		Elevation =	
ΔE [m]:			
<b>Remarks</b>			
Weather conditions:			

**Figure 21:** Example of a field survey protocol sheet used during the deployment and survey of a CR used for S-1B calibration. The relevant fields were filled in during the survey.

### 3.3.6 Photographic documentation

A recommended complement to the log (field protocol) sheet is photographic documentation of the survey/deployment. Photographs are a powerful way of recording key aspects of a survey, including:

- Processes: e.g. Which steps were taken and in what order during the various measurements? How were the various tools and measurement devices used in practice?

- Context: What objects surround a given CR? How it is oriented and set up? What type of texture does the ground/mounting surface have?
- Targets: the CRs themselves, as the main signal “generators,” should be photographed from at least two sides. Potentially important details such as the drainage hole or mounts may be photographed as well.

Besides helping to answer scientific or technical questions that may arise during later data analysis and interpretation, photographs are also useful for use in presentations and publications. As a case in point: even this report contains many photos that were originally taken for analysis/interpretation purposes.

Other than photographs focusing on particular details or processes, UZH recommends taking several photographs of the installed CRs in their larger context, from multiple viewpoints (e.g. from the four compass directions, or at minimum from the front, side and behind). This might be useful not only for reporting purposes, but to help validate the correctness of their overall and relative orientations, esp. in relation to surrounding buildings, trees, etc.

## 4 PRODUCT MONITORING DURING A SAR ACQUISITION CAMPAIGN

After the initial deployment and survey of one or more CRs intended as reference targets for a longer-term acquisition campaign, additional effort will be needed to ensure the targets remain reliable. The most predictable detrimental influences on CRs over time are rain and snowfall; both act to potentially reduce the target's RCS (rainwater may accumulate if the drainage holes become clogged; snow may cover a CR in any case). While it is possible to schedule regular site visits without regard to weather or the SAR products, it is much more efficient and economical to (a) monitor the weather conditions and (b) monitor the RCS of the imaged targets, or similarly, the SCR.

If a CR's SCR (or RCS) is measured regularly in the images acquired over a site, a "baseline" range of typical values can be established. This makes the definition of a useful threshold possible for a given target and product type. For several reasons, but most commonly rainwater and snow layers, the SCR of a CR may drop below a level considered useful. However, to determine an *evidence-based* threshold and not one purely based on statistics, information about the local weather conditions (especially precipitation) can be useful. A good example is the ambiguous case of a SAR product where the target(s) were observed to have a lower SCR than "usual," but the target was still visible in the image. Should the product be eliminated or not? The best way to make this decision – and, in the process, determine a reasonable SCR cutoff value – was by consulting the meteorological records for the time of the product, for a location near the CR(s). If it can be confirmed that there was a large amount of precipitation, a reasonable deduction is that the CR requires maintenance/cleaning as soon as possible, as complete drainage may not have occurred, especially if the drainage hole is small, or otherwise partially blocked by debris.

### 4.1 Sentinel-1 experience

In its role within the S-1 Mission Performance Centre run by the French company *Collecte Localisation Satellites* (CLS), UZH has been responsible for the geometric calibration and validation of both the S-1A and –B satellites since the launch of S-1A on 3 April 2014. Semi-automated meteorological monitoring was established for both CR sites (*Torny-le-Grand* and *Dübendorf*). This process involved two key regular observations for each received product: the target SCR and several basic meteorological measurements for stations near the test sites. In Switzerland, the national weather service (meteoswiss) operates a semi-automated network of meteorological stations whose measurements may be accessed using software they provide (for an academic licensing fee). The stations are located < 10 km from the test sites, making them quite reliable indicators of the weather at the CR sites. The quantities of interest for UZH are: temperature, relative humidity, pressure, and amount of precipitation. The first three are used for atmospheric path delay modelling; the precipitation helps determine the cause of anomalously low imaged target SCR.

**Figure 22** shows plots of the SCR and target peak intensity for all four CRs at the two Swiss test sites since S-1B launch, as imaged in IW SLC products; each target is uniquely color-coded. In (a), the SCR variation is shown over time, and in (b) it is shown as a function of ALE. The normal degree of SCR variation can be discerned from a plot such as in (a), although it is not necessarily a simple task to define a threshold for a given target. Several points are marked with dates in the figure; these are examples of products that were associated with precipitation accumulation (either rain or snow) in the reflector. A few examples led to site visits, with photographs documenting the accumulation of either rain or snow (see **Figure 18**).

In **Figure 22c**, the target peak intensity (i.e. the "signal" part of the "signal-to-clutter ratio") is plotted against the product timeline. Compared with (a), it is apparent that for a given acquisition geometry and target, the peak intensity is more stable than the SCR. This is especially clear for the UZH\_TORNY\_N/S reflectors (yellow and red points), which were larger than the others and had larger drainage holes that helped prevent rain accumulation. The UZH\_DUEB targets exhibit greater variation, esp. UZH\_DUEB\_N. Upon investigation, this was explained mainly by two factors: (1) a greater variation of elevation angles stemming from different orbital tracks, and (2) a much higher incidence of rainwater collecting in the reflectors due to objects blocking the relatively small drainage holes.

Both the SCR and peak intensity variations may be used to help determine reasonable thresholds below which further investigation is warranted. The peak intensity may be better suited to monitoring the status of the reflector independently of the background (i.e. acting as a proxy for its RCS), while the SCR is more an indicator of the target *image* quality for the purposes of geolocation estimation. That said, it is clear from **Figure 22b** that not all points below the threshold can be reliably said to correlate with precipitation issues. In other words: in some cases the SCR was low even if the measurement itself might be reliable (false-positive warnings). In the future, one

might combine estimates of the target RCS (as indicated by the peak intensity) and the SCR to better understand the role of clutter in geolocation analyses. As clutter is not a property of the target itself, it may be excluded if only the target status is of interest. However, the SCR is directly connected to the attainable geolocation accuracy, and therefore remains a useful quantity.

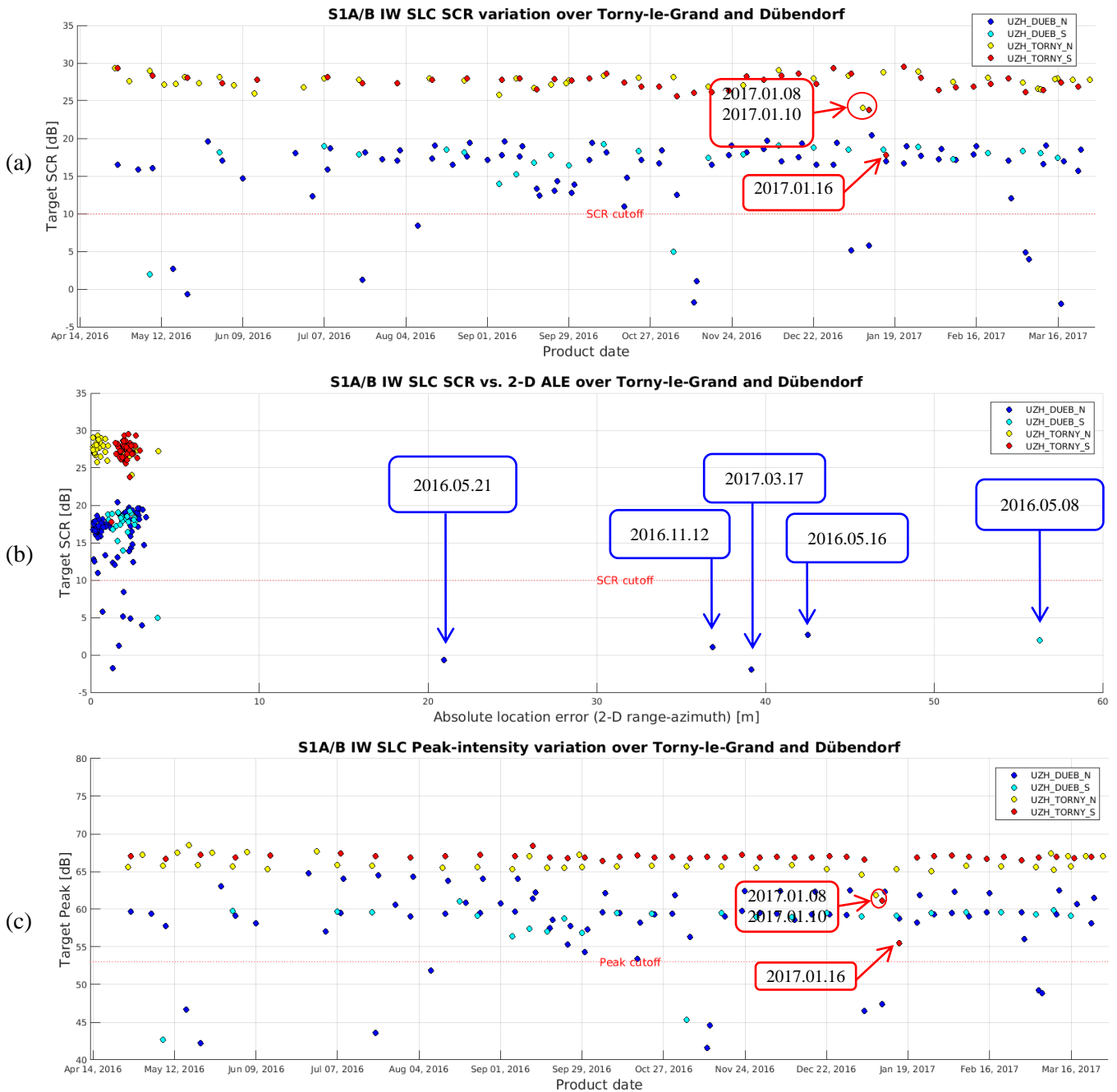


**Figure 22:** Signal to clutter ratio and peak intensity for an S-1A/B time series over Swiss corner reflectors as seen in IW SLC products (a) SCR variation over time (b) relationship between SCR and ALE. Outlier product dates indicated by arrow boxes. All five ALE outliers shown in (b) were confirmed to be caused by rain-filled CRs. The three outliers indicated in (a) were caused by partially snow-filled CRs, although the corresponding ALE was not unusually high. The dotted red line shows the 10 dB SCR threshold applied by UZH for IW SLC products over the *Dübendorf* targets.

A high target SCR in a SAR image is generally associated with high contrast and a symmetrical shape. SCR is independent of sensor-specific parameters such as imaging mode or wavelength, although the *shape* of an imaged

reflector (esp. the related quantity of spatial resolution) does depend on these things. Examples of the appearance of trihedral CRs ranging in size from 1.0-2.5 m in S-1 SM, IW and EW mode images are shown in **Figure 23**. The image extracts are not identically radiometrically scaled; they are auto-scaled to improve the CR visibility. The degree of contrast and the general shape of the CR are still clearly visible in each case.

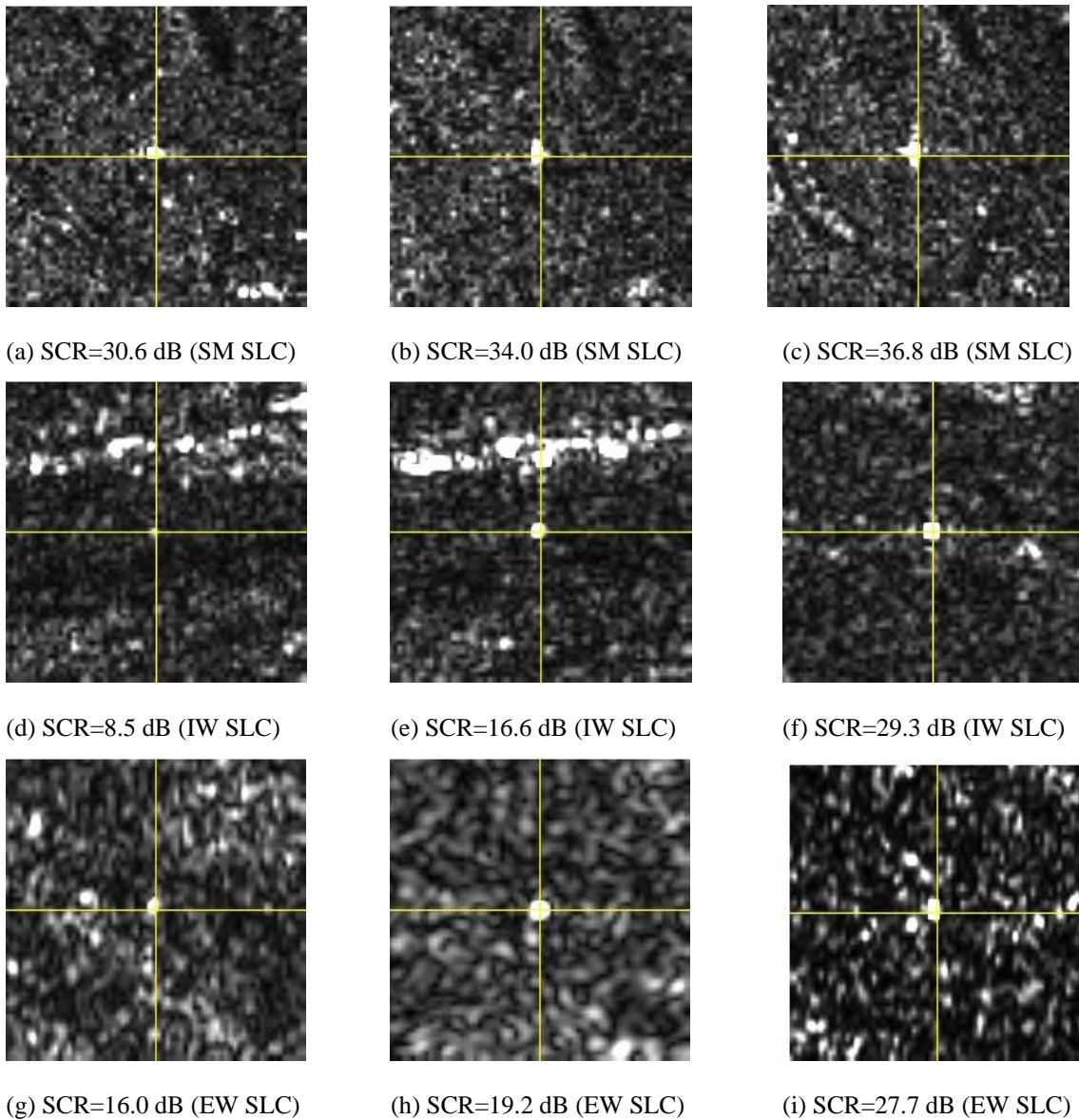


**Figure 23:** Appearance of triangular trihedral corner reflectors in S-1A/B SLC products for different SCR values. The imagettes were radiometrically auto-scaled, but their contrast relative to background and appearance of sidelobes are visibly correlated to SCR. The yellow crosses represent predicted target positions and are used as plausibility checks during ALE estimation.

- (a)-(c): SM SLC product extracts over 1.5 m CR in *Torny-le-Grand*, Switzerland
- (d)-(e): IW SLC product extracts over 1.0 m CR in *Dübendorf*, Switzerland
- (f): IW SLC product extract over 1.5 m CR in *Torny-le-Grand*, Switzerland
- (g)-(h): EW SLC product extracts over 1.5 m CR in *Torny-le-Grand*, Switzerland
- (i): EW SLC product extract over 2.5 m CR in *Surat* array, Queensland, Australia

## 4.2 TerraSAR-X experience

Analogous to **Figure 22** for S-1 IW SLC products, two examples of SCR time series of trihedral CRs using TSX high-resolution spotlight data are presented in **Figure 24**. The time series shows SCR values for the GARS O'Higgins, Antarctica, and *Metsähovi*, Finland test sites, computed according to the principles discussed in section 2.2. Two trihedral CRs with 0.7m edge length are located at GARS O'Higgins, while a single trihedral with 1.5m edge length is located at *Metsähovi*. Both sites are regularly observed by TSX and its twin, TanDEM-X (TDX), using beams with incident angles ranging from 25-54°.

For the 0.7 m CRs (theoretical peak RCS = 30.2 dBm<sup>2</sup>) at GARS O'Higgins, the average SCR is ~37 dB, see **Figure 24a**. This corresponded well with predictions, given a clutter power of -7dB and  $\beta_0 = -14$  dB. The temporal variations visible in the time series are mainly caused by the clutter variation over the course of a year. The clutter tends to be lower during the Antarctic winter due to the snow cover over the bedrock and debris (see **Figure 19c**). This background texture is exposed during the summer months, resulting in an increased clutter of ~2-3 dB for X-band. This reminds us that the natural clutter variation at the CR site has to be taken into account when defining the size of a reflector. The alignment of the CR boresight relative to the SAR viewing angle also affects the SCR (see section 2.4) and this is also clearly visible in the time series. The outliers visible in the time series were caused by snow in the reflector, which reduced the SCR to ~15 dB or less. Based on visual inspection, an empirical threshold for automatic outlier removal was set to 30 dB for the 0.7m CRs. Eight acquisitions were identified as outliers during the period before canvas protection was installed; after the installation (see section 3.3.3), only three additional acquisitions were marked as unusable as of January 2017.

The larger 1.5 m CR (nominal RCS = 43.4 dB) at *Metsähovi*, Finland, typically generates an SCR of ~52 dB (see **Figure 24b**) and the background clutter at this location remains quite homogeneous over the course of the year. The reflector is aligned with TSX beam 45, and since beam 22 deviates from this alignment by about 10.5°, its SCR values are ~1 dB lower (see **Figure 4**). Once more, several acquisitions during winter showed a significant drop in SCR, again due to snow in the reflector. The drainage hole also became clogged in the summer of 2016, resulting in a flooded CR and SCR values 20 dB or more below average. These experiments once again demonstrate that SCR monitoring is a useful monitoring tool for gauging the status of a CR, identifying the need for on-site maintenance, and for the generation of reliable ALE estimates.

Incorporation of the SCR information into the TSX ALE analysis for both test sites (details on the ALE-analysis are given in [4]) confirms that the outliers were indeed correlated to the decrease in SCR. Looking at the ALE analysis shown in **Figure 25**, one can see the correspondence between low SCR values (indicated by red symbols) and the major outliers. Many of the low-SCR acquisitions were ALE outliers, although some were not. The largest outliers, off by several meters, are marked by arrows indicating their direction (out of the plotted range); they were all correctly identified by the SCR thresholds. For some acquisitions, the lower SCR values did not translate into larger ALE. These "false positives" may be caused by thin layers of snow in the reflector which dampen the signal without affecting the signal travel time. This experiment demonstrates that not all targets exhibiting low SCR have anomalous ALE values, as was seen also for the S-1 time series (**Figure 22**).

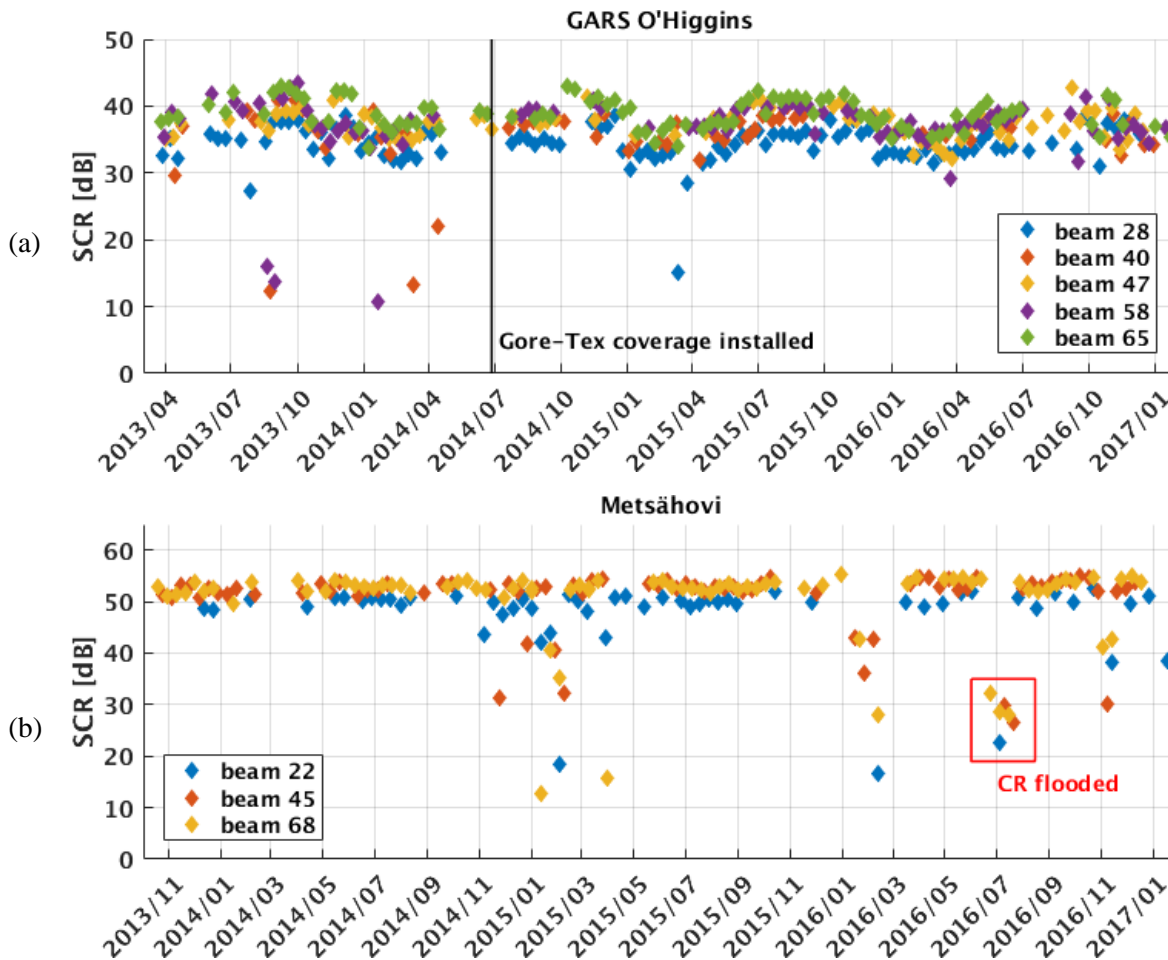
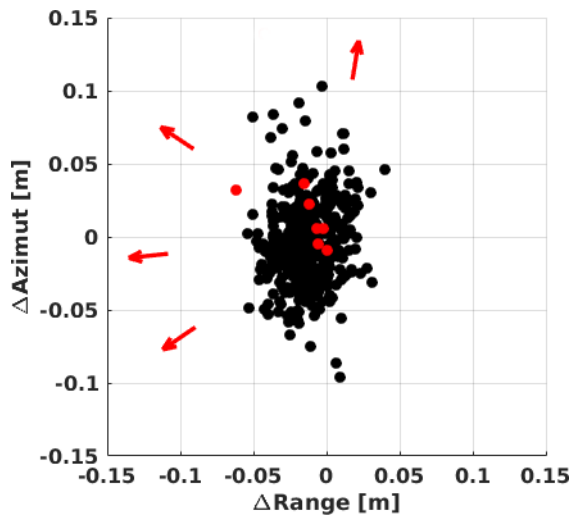
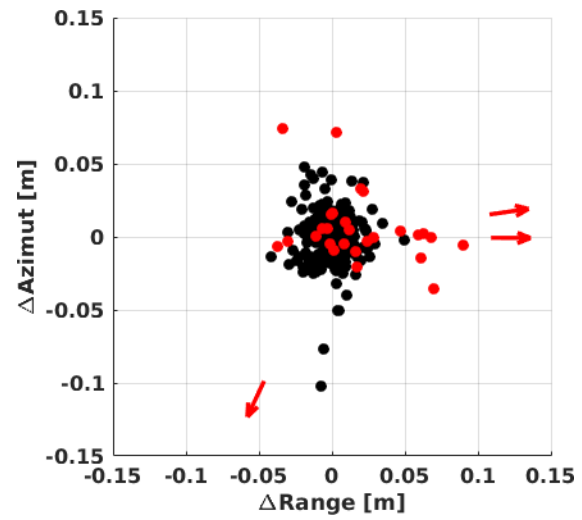


**Figure 24:** Time series of the SCR in TerraSAR-X 300 MHz high-resolution spotlight (HS300) images acquired for the reflectors at (a) GARS O'Higgins and (b) *Metsähovi*.

In spite of the above discussion, the radiometric error stemming from the low SCR is not the only possible cause of larger ALE residuals. Some of the acquisitions shown in **Figure 25** had unexpectedly large residuals in spite of the large SCR values e.g. the two outliers at the bottom of **Figure 25b**. Local perturbations in the atmosphere not captured by the corrections, or limitations in the orbital solution for the particular day, e.g. due to manoeuvres or space weather perturbations, are possible reasons for such unexpected deviations. For this reason, we recommend a sufficient number of acquisitions when performing ALE analysis, such that the identification of such outliers by statistical methods is possible. Nevertheless, the SCR analysis remains a useful tool, particularly in the context of automated data processing chains. Near-real-time processing is advised, so that quick identification of degraded CRs requiring possible maintenance can be made.



(a)



(b)

**Figure 25:** ALE scatterplot for TSX, corresponding to the data shown in **Figure 24**; (a) GARS O'Higgins (two 0.7m CRs), (b) *Metsähovi* (one 1.5m CR). The red signatures mark the outliers identified by the SCR threshold. The arrow markers point to extreme outliers also identified by the SCR, and which are outside of the plotted axis limits.

## 5 PLANNING AND DEPLOYMENT OVERVIEW

The previous chapters covered many theoretical and practical aspects of planning and executing a corner reflector deployment and survey campaign intended for spaceborne SAR geometric accuracy analysis. However, there is a core *process* that is described implicitly, one that applies especially to the deployment of trihedral CRs for geometric calibration/validation. This process, as well as major points worthy of consideration at each stage, are summarised in the following points:

- 1) Determine the necessary corner reflector size(s) (section 2.3, optionally in conjunction with Table 10-Table 13)
- 2) Select a suitable site(s) (section 2.4.1)
  - inspection of existing SAR images as a useful guide
  - large, flat open spaces preferred
  - secure/private areas preferred (may require permission from owner!)
  - clutter, nearby objects, potential multiple reflections/interference to be avoided
  - determine visibility of site(s) from known satellite tracks (e.g. use of calsky.com or similar)
- 3) Plan the CR orientation(s) (elevation & azimuthal angles; see section 2.4.2)
  - calculations for specific satellites/test sites using e.g. calsky.com
- 4) Survey the reference points and deploy the CRs (sections 3.2 and 3.3)
  - organise transport of CRs
  - prepare GPS equipment, tools, weights
  - select (and mark if needed) reference survey points
  - perform DGPS survey of survey marks
  - align CR vertex vertically roughly over survey point
  - orient the CR (elevation, azimuth angle)
  - align CR vertex vertically precisely over survey point
  - **repeat above two steps until vertical alignment and orientation are correct** (suggested tolerances: orientation angles within  $\sim 1^\circ$ , vertical alignment  $< 1$  mm horizontal error)
  - measure vertical offset of vertex above survey mark
  - add weights to the CR base
  - add weather protection if needed
- 5) Monitor and maintain the CR(s) (section 4 and, optionally, Appendix A)
  - collect SAR products
  - geometric processing
  - SCR (or RCS) monitoring
  - CR maintenance as needed, or at regular intervals

## 6 CONCLUSIONS

In this document we have provided tips and knowledge related to the deployment of corner reflectors in the field for monitoring the geometric quality of spaceborne SAR sensors. Examples were described from our experiences with Sentinel-1 and TerraSAR-X geometric calibration and validation campaigns. A high geometric calibration standard for current and upcoming radar sensors is crucial in order to enable combination of datasets from multiple tracks and multiple sensors, as well as with other geo-referenced information.

We request that readers provide any feedback they have on the document's content to: [adrian.schubert@geo.uzh.ch](mailto:adrian.schubert@geo.uzh.ch). Due to time considerations, no guarantee can be made that action will be taken in response to feedback, but all comments will be considered in the case of potential future releases of this document.

## 7 REFERENCES

- [1] AGI, Systems Tool Kit software, <http://www.agi.com/products/stk/> (accessed 16.08.2017)
- [2] Altamimi Z., Rebischung P., Métivier L. & Collilieux X., ITRF2014: A new release of the International Terrestrial Reference Frame modeling nonlinear station motions, *Journal of Geophysical Research: Solid Earth*, 121, pp. 6109–6131, 2016. doi: 10.1002/2016JB013098
- [3] Aulard-Macler M., *Sentinel-1 Product Definition*, MDA Technical Note, Ref. S1-RS-MDA-52-7440, MacDonald, Dettwiler and Associates (MDA), Richmond, BC, Canada, 2012, 126p.
- [4] Balss U., Breit H., Eineder M., Gisinger C., Schubert A., Small D., *Site Survey Protocol Definition*, DLR, TUM, UZH, Technical Note, Ref. DLR-FRM4SAR-TN-200, (*in progress*).
- [5] Balss U., Gisinger C., Cong X.Y., Eineder M., Brcic R., *Precise 2-D and 3-D Ground Target Localization with TerraSAR-X*, ISPRS - Int. Arch. Photogramm. Remote Sens. Spat. Inf. Sci., vol. XL-1/W1, no. 1, pp. 23–28, Apr. 2013.
- [6] Bamler R. & Eineder, M., *Accuracy of Differential Shift Estimation by Correlation and Split-Bandwidth Interferometry for Wideband and Delta-k SAR Systems*, *IEEE Geosci. Remote Sens. Lett.* 2, 151–155, 2005.
- [7] Curlander J. C., McDonough R. N., *Synthetic Aperture Radar: Systems and Signal Processing*, John Wiley & Sons, Inc., ISBN: 978-0-471-85770-9 672p., 1991.
- [8] Deng S., Li P., Zhang J., Yang J., *Power line detection from synthetic aperture radar imagery using coherence of co-polarisation and cross-polarisation estimated in the hough domain*. *Radar, Sonar Navig. IET* 6, 873–880, 2012.
- [9] Doerry A.W., *Reflectors for SAR Performance Testing*, Sandia National Laboratories, 57p., 2008.
- [10] Eineder M., Minet C., Steigenberger P., Cong X. & Fritz T., *Imaging Geodesy—Toward Centimeter-Level Ranging Accuracy With TerraSAR-X*. *IEEE Trans. Geosci. Remote Sens.* 49, 661–671, 2011.
- [11] EUREF Permanent GNSS Network, ETRF/ITRF Transformation, [http://www.epncb.oma.be/products\\_services/coord\\_trans/](http://www.epncb.oma.be/products_services/coord_trans/) (accessed 12.07.2017)
- [12] Freeman A., Shen Y., Werner C., *Polarimetric SAR Calibration Experiment Using Active Radar Calibrators*, *IEEE Trans. Geosci. Remote Sens.* 28, 224–240, 1990.
- [13] Freeman A., *SAR calibration: an overview*. *IEEE Trans. Geosci. Remote Sens.* 30, 1107–1121, 1992.
- [14] Fritz T., Eineder M., *TerraSAR-X Ground Segment Basic Product Specification Document*, technical note by the German Aerospace Center (DLR), Ref. TX-GS-DD-3302, Iss. 1.9, 2013.10.09, 2013. Online: <http://sss.terrasar-x.dlr.de>
- [15] Garthwaite M.C., Nancarrow S., Hislop A., Thankappan M., Dawson J.H., Lawrie S., *The Design of Radar Corner Reflectors for the Australian Geophysical Observing System*, Australian Government / Geoscience Australia, Record 2015/03 | GeoCat 82751, 2015.
- [16] Garthwaite M.C., Hazelwood M., Nancarrow S., Hislop A., Dawson J.H., *A regional geodetic network to monitor ground surface response to resource extraction in the northern Surat Basin, Queensland*, *Aust. J. Earth Sci.* 1–9, 2015. doi: 10.1080/08120099.2015.1040073
- [17] Garthwaite M. C., *On the Design of Radar Corner Reflectors for Deformation Monitoring in Multi-Frequency InSAR*. *Remote Sens.* 9, 648, 2017
- [18] Gisinger C., Willberg M., Balss U., Klügel T., Mähler S., Pail R., Eineder M., *Differential geodetic stereo SAR with TerraSAR-X by exploiting small multi-directional radar reflectors*. *J. Geod.* 91, 53–67, 2016.
- [19] Gray A. L., Vachon P. W., Livingstone C. E., Lukowski T. I., *Synthetic aperture radar calibration using reference reflectors*, *IEEE Trans. Geoscience and Remote Sensing*, 28(3), pp. 374–383, May 1990.

- [20] Hirosawa H., Matsuzaka, Y., *A Cross-Polarized SAR Image Using Dihedral Corner Reflectors*, *IEEE Trans. Geosci. Remote Sens.* **26**, 697–700, 1988.
- [21] International Association of Geodesy, Global Geodetic Observing System, <http://www.ggoc.org> (accessed 16.08.2017)
- [22] Ketelaar G., Marinkovic P., Hanssen R., *Validation of point scatterer phase statistics in multi-pass InSAR*, in Proceedings of CEOS SAR Workshop, Ulm, Germany, May 2004.
- [23] Klügel T., Höppner K., Falk R., Kühmstedt E., *Earth and space observation at the German Antarctic Receiving Station O'Higgins*, *Polar Record*, 51(6), pp. 590-610, 2015. doi: 10.1017/S0032247414000540
- [24] Land Information New Zealand (LINZ), *The 2012 Warkworth Observatory Local Tie Survey*, ITRF co-location survey: online reports, 2012. Online: [http://itrf.eng.ign.fr/local\\_surveys.php](http://itrf.eng.ign.fr/local_surveys.php)
- [25] Lauknes T.R., *Rockslide Mapping in Norway by Means of Interferometric SAR Time Series Analysis*, PHD Thesis, University of Tromsø, Department of Physics and Technology, 2010.
- [26] Lauknes T.R., Larsen Y., Rouyet L., Dehls J.F., *Monitoring of the Jettan rockslide in northern Norway using high-resolution TerraSAR-X Staring Spotlight InSAR*, Presentation held at the TerraSAR-X/TanDEM-X Science Team Meeting 2016, 2016. Online: <http://sss.terrasar-x.dlr.de>
- [27] Mahapatra P., van der Marel H., van Leijen F., Samiei-Esfahany S., Klees R., Hanssen R. InSAR datum connection using GNSS-augmented radar transponders. *J. Geod.*, 1–12, 2017. doi: DOI 10.1007/s00190-017-1041-y
- [28] Miranda N., Meadows P.J., Pilgrim A., Piantanida R., Recchia A., Giudici D., Small D., Schubert A., Sentinel -1B Preliminary Results Obtained During the Orbit Acquisition Phase [Work in Progress]. *Procedia Comput. Sci.* 2016, 100, 1313–1318. doi: 10.1016/j.procs.2016.09.247
- [29] Parker A. L. Featherstone W. E. Penna N. T. Filmer M. S. Garthwaite M. C. Practical considerations before installing ground-based geodetic infrastructure for integrated InSAR and cGNSS monitoring of vertical land motion. *Sensors (Switzerland)* 2017, 17, 1–20
- [30] Petit G., Luzum B. (eds), *IERS conventions (2010)*, Verlag des Bundesamtes für Kartographie und Geodäsie, 2010. Online: <http://tai.bipm.org/iers/conv2010/conv2010.html>
- [31] Plag H.P., Pearlman, M. (Eds.), *Global Geodetic Observing System - Meeting the Requirements of a Global Society on a Changing Planet in 2020*, Springer Berlin Heidelberg, 2009.
- [32] Qin Y., Perissin D., Lei L., *The Design and Experiments on Corner Reflectors for Urban Ground Deformation Monitoring in Hong Kong*, *International Journal of Antennas and Propagation*, vol. 2013, 2013. doi: 10.1155/2013/191685
- [33] Ray J., Altamimi, Z., *Evaluation of co-location ties relating the VLBI and GPS reference frames*, *Journal of Geodesy*, 79, pp. 189-195, 2005. doi: 10.1007/s00190-005-0456-z
- [34] Rosich B., Meadows P., *Absolute Calibration of ASAR Level 1 Products Generated with PF-ASAR*, ESA-ESRIN Technical Note, Ref. ENVI-CLVL-EOPG-TN-03-0010, Iss. 1, Rev. 5, October 2004.
- [35] Sandwell D. T., Myer D., Mellors R., Shimada M., Brooks B., Foster J., *Accuracy and resolution of ALOS interferometry: Vector deformation maps of the father's day intrusion at Kilauea*. *IEEE Trans. Geosci. Remote Sens.* **46**, 3524–3534, 2008.
- [36] Schlüter W., Zernecke R., Becker, S., Klügel T. & Thaller D., *Local Ties between the Reference Points at the Fundamentalstation Wettzell*, in IERS Technical Note No. 33: Proceedings of the IERS Workshop on site co-location, Richter B., Dick W.R., Schwegmann, W. (Eds.), pp. 64-70, 2005. Online: <https://www.iers.org/IERS/EN/Publications/publications.html>
- [37] Schneider D., Gubler E., Marti U., Gurtner W., *Aufbau der neuen Landesvermessung der Schweiz 'LV95' – Teil 3: Terrestrische Bezugssysteme und Bezugsrahmen – Bericht 8*, swisstopo, Bern, Switzerland, Feb. 2001.

- [38] Schubert A., Small D., Miranda N., *Geometric Quality Indicators for SAR Products*, Proc. CEOS SAR Calibration & Validation Workshop, 2010.
- [39] Schubert A., Small D., Miranda N., Geudtner D., Meier E., *Sentinel-1A Product Geolocation Accuracy: Commissioning Phase Results*. Remote Sens. 7, 9431–9449, 2015.
- [40] Schubert A., Small D., Meier E., Miranda N., Geudtner D., *Spaceborne SAR Product Geolocation Accuracy: a Sentinel-1 Update*, Proc. IGARSS 2014; Québec, Canada, 2014; pp. 2675–2678.
- [41] Schubert A., Small D., Jehle M., Meier E., *COSMO-SkyMed, TerraSAR-X, and Radarsat-2 Geolocation Accuracy after Compensation for Earth-System Effects*, Proc. IGARSS'12, 3301–3304, 2012.  
doi:10.1109/IGARSS.2012.6350598
- [42] Small D., *Flattening Gamma: Radiometric Terrain Correction for SAR Imagery*, IEEE Trans. Geosci. Rem. Sens., 49(8), pp. 3081-3093, August 2011. doi: 10.1109/TGRS.2011.2120616
- [43] Small D., Miranda N., and Meier, E. *A revised radiometric normalisation standard for SAR*, in International Geoscience and Remote Sensing Symposium IGARSS, Vol. IV, pp. 566–569, 2009.  
doi: 10.1109/IGARSS.2009.5417439
- [44] Small D., Rosich-Tell B., Schubert A., Meier E., Nüesch D., *Geometric Validation of Low and High-Resolution ASAR Imagery*, in ESA ENVISAT and ERS Symposium, Salzburg, Austria, 2004, 9p.
- [45] Small D., Rosich B., Meier E., Nüesch D., *Geometric Calibration and Validation of ASAR Imagery*, in CEOS WGCV SAR Calibration & Validation Workshop, 2004, 8p.
- [46] Stein S. *Algorithms for Ambiguity Function Processing*, IEEE Trans. on Acoustics, Speech and Signal Processing, Vol. ASSP-29, No. 3, June 1981.
- [47] Swerling P. *Radar Measurement Accuracy*, in *Radar Handbook*, M. Skolnik, Ed., New York, McGraw-Hill, 1970, Ch. 4.
- [48] Qin Y., Perissin D., Lei L. *The Design and Experiments on Corner Reflectors for Urban Ground Deformation Monitoring in Hong Kong*, Int. J. Antennas Propag. 2013, 8p., 2013.

## APPENDIX A: SCR AND GEOLOCATION ACCURACY

The SCR of an imaged point target (trihedral CR in our case) influences the theoretically best achievable measurement precision, as quantified by Eq. 3 in section 2.3 by limiting the precision in locating the target's main lobe. The equation reflects the connection between measurement precision (i.e. the standard deviation of an ensemble of measurements) to the signal-to-noise ratio, or the SCR in point targets imaged by SAR. Other errors influence the ALE in addition to the limitations of the estimation of the imaged peak location itself (e.g. knowledge of the orbital positions, modelled atmospheric path delay, tectonic frame shift and solid Earth tide, SAR processor-related inaccuracies). It is therefore expected *a priori* that *real* measurement series should result in ALE standard deviations *exceeding* the theoretical values given by Eq. 3 for a given imaging mode and SCR. Interestingly, this was *not* always observed to be the case, as described in the following section discussing S-1 measurement time series.

### *Sentinel-1 experience*

For S-1, several time series were collected over Swiss and Australian [14] test sites that included 1.0 m, 1.2 m, 1.5 m, 2.0 m and 2.5 m CRs. The SM, IW and EW imaging modes were all represented, with both SLC and the derivative GRD products having the highest available spatial resolution (SM GRDF, IW/EW GRDH). The SM mode series covered only a relative short period of time during the S-1A and S-1B commissioning phases, while other modes (especially IW) were collected over longer periods during S-1's routine phase.

In **Table 8**, the measured median SCR values are listed in dB for each product type, with the number of contributing products indicated in brackets. The median was chosen rather than the mean, as it better represents a typical real value for that product type, especially when outliers exist. Background colours indicate either Swiss or Australian test sites. One important limitation of the dataset exists: Especially for the 1.0 and 1.2 m CRs and SM or EW modes, the number of products available was comparatively small, limiting the statistical significance of the connected measurements for these cases. In spite of this, a couple of patterns can be observed immediately in this table: (a) the correlation between CR size and SCR, and (b) generally decreasing SCR with decreasing product spatial resolution (SM has the highest SCR, EW the lowest). Also, the measurements made over 1.5 m reflectors in Swiss and Australian sites (two central lines in the table) were quite close in most cases, as expected. An important difference between the two cases was, however, the misalignment relative to the satellite boresight axis; the misalignment was different by up to ~several degrees for the Swiss and Australian test sites.

Also in **Table 8**, one observes that the SCR for GRD products from a given acquisition mode (e.g. SM GRDF vs. SM SLC) is typically 5-6 dB lower than the SLC equivalent. This had not been expected *a priori*, as GRD products are created by projection into a ground-range geometry and resampling to reduce the spatial resolution. A brief investigation into the SCR-related calculations revealed that for GRDs, the clutter intensity estimates were proportionally *higher* for GRDs. More importantly, the GRD reflector peak intensities were significantly underestimated in comparison with the SLC-based peaks. This may be attributed to the spatial resolution loss (smoothing) during GRD generation, which affects stronger scatterers preferentially. When these effects are combined, the result is a consistently lower SCR for GRD products in comparison with their SLC equivalents.

Another apparent anomaly in **Table 8** is the higher SCR for IW SLC products over the 1.0 m CR, compared with the 1.2 m CR (a difference of 0.9 dB). This was determined to be caused by a larger mean clutter in the product time series over the 1.2 m CR, despite the fact that both CRs were placed within metres of each other. The result reminds us that SCR requires careful interpretation, and in some cases, target peak intensity may be preferred.

**Table 8: Measured median SCR values [dB] over CRs in Sentinel-1 products, with the number of contributing products (sometimes observed from multiple tracks) in brackets. Values are based on observations at test sites in Switzerland (CH) and the *Surat* array in Australia (AU). N.B. alignment of the CR boresight with the sensor was only possible to within  $\sim 10^\circ$ , esp. over the CH sites. In such cases, the values under-represent the best possible SCR for these target/product combinations by up to  $\sim 1$  dB. Values marked N/A are not available.**

Triangular tri-hedral CR size [m]	SM SLC	SM GRDF	IW SLC	IW GRDH	EW SLC	EW GRDH
2.5 (AU)	44.6 (3)	38.8 (2)	38.8 (50)	32.6 (57)	27.3 (42)	22.3 (6)
2.0 (AU)	40.7 (3)	34.7 (2)	34.8 (50)	28.4 (56)	22.9 (42)	18.0 (6)
1.5 (AU)	35.4 (6)	28.1 (2)	29.7 (91)	23.7 (110)	17.8 (42)	12.9 (6)
1.5 (CH)	35.0 (25)	29.6 (25)	27.7 (85)	21.9 (74)	17.9 (27)	13.8 (27)
1.2 (CH)	30.4 (6)	25.0 (5)	17.2 (68)	14.4 (58)	10.2 (12)	6.4 (10)
1.0 (CH)	27.8 (6)	21.3 (6)	18.1 (24)	11.3 (21)	9.4 (4)	N/A

**Table 9** provides a comparison between the theoretical “lower limit” standard deviation given by SCR (using Eq. 3), and actual measured ALE standard deviations in each image dimension. The comparisons are separated by CR size, test site and product type. The most obvious pattern is indicated by the font colours. When the measured standard deviation was *at least as large as the theoretical limit*, it is coloured green. Measurement values *smaller than the theoretical limit* are highlighted red, as these are unexpectedly low (measurement precision *better* than theory). The colouring reveals a general pattern: measurements tend to become unexpectedly better than theory with decreasing CR size (i.e. towards the bottom of the table) and increasing spatial resolution (i.e. towards the right side of the table). Both of these observations may relate more directly to a single variable: the SCR itself. A bold line in **Table 9** is shown separating the “expected” and “unexpected” relationships between theory and measurement. The corresponding line is (approximately) indicated in **Table 8**, although the separation between range and azimuth dimensions is not reflected here. However, it is nonetheless apparent that the thick line corresponds to an SCR value of  $\sim 23$  dB in **Table 8**. Above this value, the measured precision was worse than the theoretical limit (as expected), but below this cutoff the relationship was no longer observed to be valid. Of course, it is not a binary choice of either “valid” or “invalid.” Rather, a trend of ever-increasing disparity between measurement and theoretical limit was observed, roughly progressing from high resolution products over large CRs to low-resolution products over smaller CRs. One could conclude that for Eq. 3 to be considered valid, an  $SCR > \sim 23$  dB is needed. The idea of a threshold limiting the validity of Eq. 3 was already suggested by one of the authors who originally described the theory; in section III in [46], the author writes that a 10 dB SCR is needed for unambiguous lobe peak identification. However, no constraints were described that would limit the validity of the equation beyond this. Moreover, the variability of the relationship between theory and measurement reminds us that other influences are at work - in particular, some may be related to specific aspects of the S-1 system and processor.

For cases where the measured ALE standard deviation was larger than the SCR-based theoretical value (i.e. as expected), the most straightforward interpretation of the variable difference is that the SCR contributes to the total imprecision to a greater or lesser degree. Other non-CR-related quantities of variable quality include the atmospheric model quality (affecting path delay estimation), the tectonic and solid Earth tide models, the quality of the orbital positions and processor-specific issues.

Even with these known limitations in mind, and keeping in mind that these values are specific to S-1, one must still conclude that the theoretical relationship between SCR and geolocation precision (Eq. 3) cannot be considered valid in all cases. If it were, no examples of measured standard deviation lower than the theoretical deviation should be found. This is all the more true as any further variable influences (known or unknown) would be expected to increase the standard deviation, not decrease it.

**Table 9: Theoretical (Theo) and measured (Meas) ALE standard deviation contributions** in [m] corresponding to SCR values in previous table, i.e. for Sentinel-1 products. Theoretical values generated using Eq. 3; measured values taken from calibration/validation campaigns over Swiss (CH) and Australian (AU) targets. **Red** values indicate measured values that are (unexpectedly) *better* than their theoretical counterparts; **green** values are equal to or worse than theory (as expected). Values marked N/A are not available.

Triangular trihedral CR size [m]		SM SLC		SM GRDF		IW SLC		IW GRDH		EW SLC		EW GRDH	
		rg	az	rg	az	rg	az	rg	az	rg	az	rg	az
2.5 (AU)	Theo	0.01	0.01	0.04	0.04	0.01	0.10	0.18	0.19	0.20	0.73	1.52	1.47
	Meas	0.04	0.12	0.24	0.30	0.27	0.21	0.36	0.92	0.26	0.63	0.4	1.07
2.0 (AU)	Theo	0.01	0.01	0.06	0.06	0.02	0.15	0.30	0.32	0.33	1.21	2.51	2.42
	Meas	0.11	0.08	0.25	0.20	0.32	0.25	0.40	0.84	0.41	0.95	0.56	1.09
1.5 (AU)	Theo	0.02	0.02	0.14	0.14	0.04	0.28	0.18	0.19	0.59	2.19	4.48	4.32
	Meas	0.04	0.09	0.15	0.19	0.24	0.87	0.29	1.02	0.53	2.12	0.81	2.40
1.5 (CH)	Theo	0.02	0.02	0.11	0.11	0.05	0.35	0.63	0.67	0.59	2.17	4.07	3.92
	Meas	0.07	0.28	0.22	0.26	0.10	0.97	0.21	1.01	0.48	3.71	0.96	3.55
1.2 (CH)	Theo	0.03	0.04	0.19	0.19	0.17	1.17	1.49	1.59	1.41	5.21	9.54	9.20
	Meas	0.03	0.04	0.04	0.45	0.12	1.37	0.29	1.44	0.67	2.67	1.42	2.36
1.0 (CH)	Theo	0.04	0.06	0.30	0.30	0.15	1.05	2.13	2.26	1.56	5.76	N/A	N/A
	Meas	0.04	0.08	0.14	0.06	0.08	0.48	0.26	0.75	0.44	2.08	N/A	N/A

The SCR values provided in **Table 8** are not simple to interpret, as the CRs were oriented towards a “mean” elevation for all planned satellite tracks. In order to provide a pair of tables similar to **Table 8** and **Table 9**, but with better comparability between modes and product types, a new set of values was created using these as a basis. The values were adjusted to compensate for the mean misalignment. Those adjusted results are listed in **Table 10**, where the *difference* between the mean incident angle at a target and the CR incident angle was used to estimate a rough SCR *inflation* factor. The approximation made is that 10° of misalignment corresponds to 1 dB of SCR reduction (see **Figure 4**); between 0 dB and 1 dB, linear interpolation was performed as a first approximation. Also, mean incident angles for a given site and CR size were used for the correction of the mean SCR value in each case, which is not exactly correct. A more accurate normalisation would be based on product-by-product and target-by-target adjustment, but these numbers were not readily available and the differences were not expected to be large.

Comparing the SCR values for the Swiss and Australian 1.5 m CRs in **Table 10**, we see that differences between them range from 0.2 dB (EW GRDH) to 1.9 dB (IW SLC). These differences were much smaller than SCR differences for CRs of different sizes, but are still not insignificant. There is a straightforward explanation: as the SCR is a combined measure of reflector RCS and local clutter, the SCR differences are mainly due to clutter differences at the two sites. For reasons that are not yet fully understood, the measured clutter RCS was often higher at the Swiss sites than in Australia, in spite of the asphalt or concrete immediately surrounding the CRs in Switzerland. It may be that the clutter calculation (as described in section 2.2) for Swiss sites was factoring nearby bright targets into the mean; the concrete/asphalt at both sites only extends to the local neighbourhood. Beyond this, there are grassy slopes and various small buildings. The Australian CRs are generally located in isolated, flat and dry areas. These factors may explain the higher mean RCS in the Switzerland images. Even if this is the case, the clutter immediate-

ly surrounding the targets may in fact be lower at Swiss sites, but the clutter *measurement* is not limited to the nearest samples, as statistically relevant values required larger regions.

With the limitations described above in mind, **Table 10** nonetheless represents a good sampling of typical SCR values that may be expected for different CR sizes and S-1 product modes/types, given good alignment between the CR boresight and the sensor. Since the values are based on measurements and rescaled to boresight using a first-order approximation approach, the SCR values should not be considered accurate to better than  $\sim 0.5$  dB.

The theoretical lower-limit contributions of the SCR to the geolocation precision for the SCR values from **Table 10** are listed in **Table 11**, again based on Eq. 3. As discussed above, the values provided here do not reflect true ALE standard deviations, but only theoretical values based on SCR alone. The actual ALE measured from the data may be better than the theoretical predictions, especially for smaller CRs and coarser product types (i.e. for lower SCR).

**Table 10:** Boresight-adjusted median SCR values [dB] measured over CRs in S-1 products. Values are based on observations at test sites in Switzerland (CH) and the *Surat* array in Australia (AU), but have been inflated to roughly compensate for misalignment between the CR boresight and the sensor direction ( $+1$  dB /  $10^\circ$  of misalignment). Values marked N/A are not available.

Triangular tri- hedral CR size [m]	SM SLC	SM GRDF	IW SLC	IW GRDH	EW SLC	EW GRDH
2.5 (AU)	45.2	39.2	39.1	32.9	28.4	23.4
2.0 (AU)	41.3	35.1	35.1	28.7	24.0	19.0
1.5 (AU)	36.0	28.6	29.8	23.8	18.9	14.1
1.5 (CH)	35.2	29.8	27.9	22.1	18.0	13.9
1.2 (CH)	30.4	25.1	18.7	15.9	10.7	6.7
1.0 (CH)	27.8	21.3	19.1	12.4	9.4	N/A

**Table 11:** Theoretical geolocation standard deviation contribution in [m] based on SCR values in **Table 10**, generated using Eq. 3. Values marked N/A are not available.

Triangular tri-hedral CR size [m]	SM SLC		SM GRDF		IW SLC		IW GRDH		EW SLC		EW GRDH	
	rg	az	rg	az	rg	az	rg	az	rg	az	rg	az
2.5 (AU)	0.01	0.01	0.04	0.04	0.01	0.09	0.18	0.19	0.17	0.65	1.35	1.30
2.0 (AU)	0.01	0.01	0.06	0.06	0.02	0.15	0.29	0.31	0.29	1.07	2.22	2.14
1.5 (AU)	0.02	0.02	0.13	0.13	0.04	0.27	0.18	0.19	0.52	1.92	3.93	3.79
1.5 (CH)	0.02	0.02	0.11	0.11	0.05	0.34	0.62	0.65	0.58	2.13	4.00	3.86
1.2 (CH)	0.03	0.04	0.19	0.19	0.14	0.98	1.25	1.33	1.34	4.97	9.15	8.82
1.0 (CH)	0.04	0.06	0.30	0.30	0.13	0.94	1.89	2.00	1.56	5.76	N/A	N/A

### *TerraSAR-X experience*

**Table 12** lists typical SCR values for the trihedral CRs of different sizes in X-band, based on real TSX acquisitions. Note that the *mean* values were calculated here; for S-1, the *medians* were computed (**Table 8** and **Table 10**). The difference between the two was seen to be nearly negligible if no large outliers exist; also, these tables are only intended to provide typical values. The values are linked to the different TSX imaging modes and were computed from sets of level 1B slant range products [14] according to the procedures documented in section 2.2.

Using the nominal resolution of the products, the SCR can be converted to ALE standard deviation contribution in range and azimuth, i.e. the contribution to the precision stemming entirely from the image radiometry; see Eq. 3 in section 2.3. Applying this conversion to the values of **Table 12** yields the theoretical results shown in **Table 13** in the rows labelled “Theo.” The measured standard deviations are listed in the adjacent rows labelled “Meas.” The standard deviations describe the ALE spread within the scatter “clouds” and reflect the variability experienced when using different beams (incident angles) for a CR having a fixed orientation, as well as the variability induced by seasonal changes in the clutter (ground backscatter). Looking at the table, one can see that these contributions can change the typical SCR values of a CR up to ~2.6 dB. The expected ALE standard deviation due to the SCR is at the millimetre or even sub-millimetre level. In contrast to this, other effects such as the limited orbital knowledge and signal propagation delay model errors contribute significantly more to the overall ALE of about 1–2 cm.

Although few comparisons between measured and theoretical precision are currently available for TSX (two reflector sizes and two product types), a comparison may be drawn between **Table 8** (S-1) and **Table 12** (TSX) in parallel with **Table 9** and **Table 13**. The TSX SCR values are significantly higher for the 1.5 m CR, but the 0.7 m CR, with its SCR of 37 dB (HR-SL products) is comparable to S-1 SM SLC product SCR over 1.5 m and 2.0 m CRs. In both cases, the theoretical values are significantly lower than the measured ones (as expected). The difference is even larger for TSX products acquired over the 1.5 m CR. These large differences may indicate that the SCR contribution to the *total* measurement uncertainty decreases proportionally with increasing SCR, although this can only be a tentative conclusion given the limitations of the current study.

**Table 12: Mean SCR values [dB] measured over CRs in TSX SSC products, with the number of contributing products in brackets. Values are based on observations at test sites in Germany (DE) and at the Antarctic Peninsula (ANT). Note that boresight alignment was not always possible, so some values under-represent the maximum possible SCR for these target/product combinations. ST-SL = staring spotlight, HR-SL = high-resolution spotlight**

Triangular CR size [m]	triangular	ST-SL	HR-SL
1.5 (DE)		56.7 (18)	52.2 (271)
0.7 (ANT)		*	37.0 (403)

\*=no ST-SL acquisitions available from this test site

**Table 13: Theoretical (Theo) and measured (Meas) ALE standard deviations in [mm] corresponding to SCR values in previous table. Theoretical values generated using Eq. 3 and the nominal (rg x az) resolutions of the TSX SLC products [14]: staring spotlight (0.6 x 0.25 m), high-resolution spotlight (0.6 x 1.1 m). Measured values were taken from calibration/validation experiments over German (DE) and Antarctic (ANT) targets. Green values are equal to or worse than theory (as expected). Values marked N/A are not available.**

Triangular CR size [m]		ST-SL		HR-SL	
		rg	az	rg	az
1.5 (DE)	Theo	0.3	0.1	0.6	1.0
	Meas	14.1	17.7	11.6	18.8
0.7 (ANT)	Theo	1.7	0.6	3.3	6.0
	Meas	N/A	N/A	16.2	27.5

\*= no ST-SL acquisitions available from this test site